



GomSpace Aps
Langagervej 6
9220 Aalborg E

JUVENTAS MISSION ANALYSIS REPORT (MAR)

Juventas Cubesat for Hera

Reference: JUV-GS-MAR-001

Version: 1.0

Date: 2019-07-05

Document Title:	Juventas Mission Analysis Report (MAR)		
Document Reference:	JUV-GS-MAR-001		
Document Version:	1.0	Date:	2019-07-05
Abstract			

Approval Table:

Action	Name	Function	Signature	Date
Prepared by:	Hannah Goldberg	Systems Engineer		2019-07-05
Verified by:	H. Goldberg	Project Manager		2019-07-05
Approved by:	H. Goldberg	Project Manager		2019-07-05

Authors and Contributors:

Name	Contact	Description	Date
Hannah Goldberg	hrg@gomspace.com	System Engineer	2019-07-05
Claudiu Prioroc	cprioroc@gmv.com	GNC Lead	2019-07-05
GMV-RO GNC team		Mission analysis team	

Document Change Log

Issue	Date	Description
0.1	2018-10-23	First draft
0.2	2019-03-21	Coverage analysis added
1.0	2019-07-05	Launch, commissioning, baseline SSTO at 3.3 and 2.0 km, and landing selected. Delta-V budget and mission profile added. Radar analysis added.

TABLE OF CONTENTS

1. INTRODUCTION.....	1
1.1 PURPOSE.....	1
1.2 SCOPE.....	1
2. REFERENCES	2
2.1 APPLICABLE DOCUMENTS	2
2.2 REFERENCE DOCUMENTS	2
3. ACRONYMS	4
4. MISSION DESIGN	6
4.1 REFERENCE FRAMES	6
4.2 CUBESENT AND DYNAMIC PARAMETERS.....	8
4.3 MISSION PROFILE.....	9
4.3.1 Orbit and Pointing Profiles.....	10
5. MISSION ANALYSIS.....	11
5.1 LAUNCH, COMMISSIONING ORBIT, AND TRANSFER PHASE (CP AND TP).....	11
5.1.1 Release and Commissioning	11
5.1.2 Training Orbit	14
5.1.3 Transfer Phase.....	15
5.2 OBSERVATIONS PHASES (GOP AND POP).....	17
5.2.1 Proposed Orbits.....	17
5.2.2 Coverage Analysis.....	18
5.2.3 Global Observations Phase (GOP)	29
5.2.4 Proximity Observations Phase (POP).....	31
5.2.5 Complete Coverage during the Observations Phases	33
5.3 LANDING PHASE (LP) TRAJECTORY SELECTION.....	34
5.3.1 Analysis on Touchdown Velocity	35
5.3.2 Landing Trajectory	43
5.4 PAYLOAD OPERATIONS PLANNING AND ANALYSIS.....	53
5.4.1 Radar Observations.....	53
5.4.2 Radio Science	54
5.4.3 Gravimeter	54
5.5 MISSION DELTA-V BUDGET.....	54
5.6 COMMUNICATION “ACCESSES” VIA ISL.....	55
6. CONCLUSIONS	58

TABLE OF TABLES

TABLE 4-1 JUVENTAS CUBESAT CONSIDERED PARAMETERS	8
TABLE 4-2 DIDYMON CONSIDERED PARAMETERS	9
TABLE 4-3 MISSION TIMELINE NOMINAL CASE	10
TABLE 5-1. SSTO-DIDYMAIN FOR DIDYMOON RESONANT PERIODS (IN ORANGE ARE SELECTED ORBITS FOR THE COVERAGE ANALYSIS).....	19
TABLE 5-2. SSTO-DIDYMAIN FOR DIDYMAIN RESONANT PERIODS (IN ORANGE, SELECTED ORBITS FOR THE COVERAGE ANALYSIS).....	20
TABLE 5-3. DIDYMOON COVERAGE FOR A MESH OF RADIUS AND DURATIONS (IN ORANGE, TWO RESONANT ORBITS). .	23
TABLE 5-4. DIDYMAIN COVERAGE FOR A MESH OF RADIUS AND DURATIONS.	28
TABLE 5-5 SURFACE COVERAGE DURING THE OBSERVATIONS PHASES	33
TABLE 5-6 LANDING STUDY AT LANDING VELOCITY OF 6CM/S.	35
TABLE 5-7 LANDING STUDY AT LANDING VELOCITY OF 7 CM/S.....	37
TABLE 5-8 LANDING STUDY AT LANDING VELOCITY OF 8 CM/S.....	39
TABLE 5-9 LANDING STUDY AT LANDING VELOCITY OF 9 CM/S.....	40
TABLE 5-10 LANDING STUDY AT LANDING VELOCITY OF 10 CM/S.....	42
TABLE 5-11 TRANSLATIONAL DELTA-V BUDGET [CM/S] AND MARGINS AS PER [AD-8].	54

TABLE OF FIGURES

FIGURE 4-1. SCHEMATIC OF THE INERTIAL FRAMES IN USE.	7
FIGURE 4-2 HERA SC - DEPLOYER ON THE +Z FACE	7
FIGURE 4-3 JUVENTAS CUBESAT REFERENCE FRAME	8
FIGURE 4-4 SCHEMATIC OF THE JUVENTAS CUBESAT.....	9
FIGURE 5-1. HERA'S NOMINAL ATTITUDE SCHEMATIC.	12
FIGURE 5-2 JUVENTAS AND HERA – RELEASE ORBIT – TRAJECTORY, DISTANCE, VELOCITY MARGIN, AND PHASE ANGLE	14
FIGURE 5-3 JUVENTAS – RELEASE AND TRAINING ORBIT – TRAJECTORY, DISTANCE, VELOCITY MARGIN, AND PHASE ANGLE	15
FIGURE 5-4 JUVENTAS – TRANSFER TO SSTO – TRAJECTORY, DISTANCE, VELOCITY MARGIN, VELOCITY, AND PHASE ANGLE	17
FIGURE 5-5 SCHEMATIC OF AN SSTO	17
FIGURE 5-6 SSTO PERIOD AS A FUNCTION OF THE DISTANCE TO DIDYMAIN.....	18
FIGURE 5-7. SCHEMATIC OF THE VISIBILITY CONDITIONS OF THE JUVENTAS CUBESAT.	19
FIGURE 5-8. DIDYMAIN SHADOW ON DIDYMOON'S GROUND TRACK.	23
FIGURE 5-9. DIDYMOON GROUND TRACK FOR A 1.5 KM SSTO FOR 60 DAYS.	23
FIGURE 5-11. DIDYMOON GROUND TRACK OF A RESONANT SSTO.	25
FIGURE 5-12. DIDYMOON GROUND TRACK OF A NON-RESONANT SSTO.....	25
FIGURE 5-10 DIDYMOON COVERAGE VS TIME	26

FIGURE 5-13. SCHEMATIC OF THE UNOBSERVABILITY OF THE POLES OF DIDYMAIN	27
FIGURE 5-14. DIDYMAIN GROUND TRACK OF A 7 KM SSTO FOR 60 DAYS	27
FIGURE 5-15. DIDYMAIN GROUND TRACK OF A 3 KM SSTO FOR 60 DAYS	28
FIGURE 5-16 DIDYMAIN COVERAGE VS TIME.....	29
FIGURE 5-17. 3.3 KM SSTO IN SYNODIC (LEFT) AND ECLIPTIC (RIGHT).....	30
FIGURE 5-18 DIDYMOON GROUND TRACK DURING THE GLOBAL OBSERVATIONS PHASE SSTO 3.3 KM	31
FIGURE 5-19 DIDYMAIN GROUND TRACK DURING THE GLOBAL OBSERVATIONS PHASE SSTO 3.3 KM	31
FIGURE 5-20. 2 KM SSTO IN SYNODIC (LEFT) AND ECLIPTIC (RIGHT).....	32
FIGURE 5-21 DIDYMOON GROUND TRACK DURING THE GLOBAL OBSERVATIONS PHASE SSTO 3.3 KM	33
FIGURE 5-22 DIDYMAIN GROUND TRACK DURING THE GLOBAL OBSERVATIONS PHASE SSTO 3.3 KM	33
FIGURE 5-23 DIDYMOON GROUND TRACK DURING THE GLOBAL OBSERVATIONS PHASE SSTO 3.3 KM	34
FIGURE 5-24 DIDYMAIN GROUND TRACK DURING THE GLOBAL OBSERVATIONS PHASE SSTO 3.3 KM	34
FIGURE 5-25 LANDING SITES AT A 6CM/S LANDING VELOCITY AT 28-JULY-2027 19:15:00.....	37
FIGURE 5-26 LANDING SITES AT A 7 CM/S LANDING VELOCITY AT 29-JULY-2027 02:15:00.....	38
FIGURE 5-27 LANDING SITES AT A 8 CM/S LANDING VELOCITY AT 29-JULY-2027 23:15:00.....	40
FIGURE 5-28 LANDING SITES AT A 9 CM/S LANDING VELOCITY AT 28-JULY-2027 18:15:00.....	41
FIGURE 5-29 LANDING SITES AT A 10 CM/S LANDING VELOCITY AT 29-JULY-2027 04:15:00.....	43
FIGURE 5-30 LANDING SITES AT A 9 CM/S LANDING VELOCITY AT 28-JULY-2027 18:15:00.....	44
FIGURE 5-31 LANDING TRAJECTORIES AT A 9 CM/S LANDING VELOCITY AT 28-JULY-2027 18:15:00, ONLY THE 8 HOURS PRIOR LANDING ARE PLOT.....	44
FIGURE 5-32 PHASE ANGLES ANALYSIS FOR THE SELECTED LANDING AT A 9 CM/S LANDING VELOCITY AT 28-JULY-2027 18:15:00.....	45
FIGURE 5-33 SELECTED LANDING AT A 9 CM/S LANDING VELOCITY AT 28-JULY-2027 18:15:00.....	46
FIGURE 5-34 MAXIMUM CoR ALLOWED TO ENSURE A FUTURE REBOUND IN DIDYMOON SURFACE AFTER THE INITIAL LANDING TOUCHDOWN FOR THE LANDING AT 9 CM/S AT 28-JULY-2027 18:15:00.....	47
FIGURE 5-35 SELECTED LANDING AT A 9 CM/S LANDING VELOCITY AT 28-JULY-2027 18:15:00 AND POSTERIOR REBOUND AFTER REACHING THE DIDYMOON SURFACE AGAIN.....	48
FIGURE 36: RADAR OBSERVATION NUMBER OF REVISITS ACROSS DIDYMOON (MIN=7, MAX=54).....	54
FIGURE 5-37 JUVENTAS-HERA RANGE DURING THE GOP	56
FIGURE 5-38 JUVENTAS-HERA LINE OF SIGHT ANGLE W.R.T ISL PAYLOAD DURING THE GOP	56
FIGURE 5-39 JUVENTAS-HERA RANGE DURING THE POP	57
FIGURE 5-40 JUVENTAS-HERA LINE OF SIGHT ANGLE W.R.T. ISL PAYLOAD DURING THE POP	57

1. Introduction

1.1 Purpose

This document describes the analysis performed in support of the mission planning prior to launch

1.2 Scope

The present document applies to the Juventas 6U CubeSat in support of the Hera mission.

2. References

2.1 Applicable documents

Ref.	Document Title	Issue and Revision, Date
[AD-1]	Hera CubeSat Requirements	1.0
[AD-2]	CubeSat DIL	iss1 rev2
[AD-3]	CubeSat DRD	iss1 rev3
[AD-4]	Space Debris Mitigation Policy for Agency Projects	2014 002e
[AD-5]	CubeSat Design Specification	rev13
[AD-6]	CubeSat ECSS Eng. Tailoring	iss1 rev3
[AD-7]	CubeSat PQA Reqts	iss1 rev1
[AD-8]	CubeSat Margin Policy	iss1 rev0
[AD-9]	CubeSat Review Objectives	iss1 rev1

2.2 Reference documents

Ref.	Document Title	Issue and Revision, Date
[RD-1]	ASCOT2 – A small body lander to investigate the interior of 65803 Didymos' moon in the frame of the AIDA/AIM mission	Acta Astronautica 149 (2018) 25–34
[RD-2]	Reliability Analysis of Ballistic Landing in Binary Asteroid 65803 (1996GT) Didymos under Uncertainty and GNC Error Considerations.	ISTS-2017-d-031 / ISSFD-2017-031
[RD-3]	Hera - Payload Interfaces	Issue 1.5
[RD-4]	Juventas GNC Analysis Report	v0.2
[RD-5]	Scheeres, D., Sutter, B. and Rosengren, A. (2013), "Design, dynamics and stability of the osiris-rex sunterminator orbits", Advances in the Astronautical Sciences Vol. 148, pp. 3263–3282.	
[RD-6]	Hussmann, H., Oberst, J., Wickhusen, K., Shi, X., Damme, F., Lüdicke, F., Lupovka, V. and Bauer, S. (2012), "Stability and evolution of orbits around the binary asteroid 175706 (1996 fg3): Implications for the marcopolor mission", Planetary and Space Science Vol. 70 nr. 1, pp. 102 – 113.	
[RD-7]	Juventas Mission Requirements Document (MRD)	v0.1
[RD-8]	MASCOT2 – A small body lander to investigate the interior of 65803 Didymos' moon in the frame of the AIDA/AIM mission	Acta Astronautica 149 (2018) 25–34

Ref.	Document Title	Issue and Revision, Date
[RD-9]	Reliability Analysis of Ballistic Landing in Binary Asteroid 65803 (1996GT) Didymos under Uncertainty and GNC Error Considerations.	ISTS-2017-d-031 / ISSFD-2017-031

3. Acronyms

Acronyms	Description
AD	Applicable Document
ADCS	Attitude Determination and Control System
AKE	Absolute Knowledge Error
CoR	Coefficient of Restitution
CS	CubeSat
DCP1	Detailed Characterization Phase – before PDP
DCP2	Detailed Characterization Phase – after PDP
DDVV	Development, Design, Validation and Verification
DKE	Dynamic and Kinetic Environment
DOF	Degree of Freedom
ECP	Early Characterization Phase
ECSS	European Cooperation for Space Standardization
EKF	Extended Kalman Filter
EOL	End of Life
EPS	Electronic Power System
ERN	Enhanced Relative Navigation
FDIR	Failure detection Isolation and recovery
GNC	Guidance, Navigation and Control
GNC ASW	GNC Application Software
HIL	Hardware in the Loop
HW	Hardware
IP	Image Processing
IP-ICU	Image Processing and Instruments Control Unit
ISL	Inter-Satellite Link
MIL	Model in the Loop
MOC	Mission Operations Centre
MSRD	Mission and System Requirements Document
MVM	Mode Vehicle Management
OBSW	On-board Software
ODCS	Orbit Determination and Control system
PDF	Probability Density Function
PDP	Payload Deployment Phase
PDR	Preliminary Design Review
RCS	Reaction Control System
RD	Reference Document
RW	Reaction Wheel
RWA	Reaction Wheel Assembly
SC	Spacecraft
SDR	Software Defined Radio
SMA	Semi-Major Axis
SNR	Signal to Noise Ratio
SRP	Solar radiation Pressure
SSTO	Self-Stabilized Terminator Orbit

Acronyms	Description
STR	Star Tracker
SW	Software
TBC	To Be Confirmed
TBD	To Be Determined
TMTC	Telemetry and Telecommand
UKF	Unscented Kalman Filter

4. Mission Design

4.1 Reference Frames

- **Didymain-Didymoon Rotating Frame** is a non-inertial mid step frame used to convert quantities that are referred to Didymoon
 - **Origin** Didymain's center of mass.
 - **X-Axis** Vernal equinox.
 - **Y-Axis** Completes the right-handed system.
 - **Z-Axis** Didymain's pole.
- **Didymain Body-fixed Frame** is a non-inertial frame, useful to compute characteristics that are fixed to Didymain's body.
 - **Origin** Didymain's center of mass
 - **X-Axis** Arbitrary direction orthogonal to Z-axis and kept fixed to Didymain.
 - **Y-Axis** Completes the right-handed system.
 - **Z-Axis** Didymain's rotation axis.
- **Didymoon Body-fixed Frame** is a non-inertial frame with the same purpose than the Didymain Body-fixed Frame but for Didymoon.
 - **Origin** Didymoon's center of mass.
 - **X-Axis** Pointing to Didymain
 - **Y-Axis** Completes the right-handed system.
 - **Z-Axis** Didymoon's rotation axis parallel to Didymain's pole due to Didymain and Didymoon are tidally locked.
- **Didymos-sun Synodic Frame** is a non-inertial frame useful for the computation of the self-stabilized terminator orbits.
 - **Origin** Didymain's center of mass.
 - **X-Axis** Sun direction.
 - **Y-Axis** Completes the right-handed system.
 - **Z-Axis** Parallel to the Heliocentric momentum of Didymos Orbit.
- **CubeSat Body Frame** is fixed to the spacecraft, as per Figure 4-3.
 - **Origin** CubeSat center-of-mass.
 - **X-Axis** Asteroid bore-sight direction, camera and laser altimeter
 - **Y-Axis** Direction of the solar arrays, completes the right-handed system
 - **Z-Axis** Deployment axis
- **HERA Body Frame** is fixed to the spacecraft, as per Figure 4-2.
 - **Origin** HERA center-of-mass.
 - **X-Axis** High-gain antenna
 - **Y-Axis** Solar arrays

- **Z-Axis** Camera boresight and deployer.
- **Camera Body Frame** simulate the camera images as used by the navigation system.
 - **Origin** Center of the camera sensor
 - **X-Axis** Horizontal axis of the camera sensor
 - **Y-Axis** Vertical axis of the camera sensor
 - **Z-Axis** Boresight direction

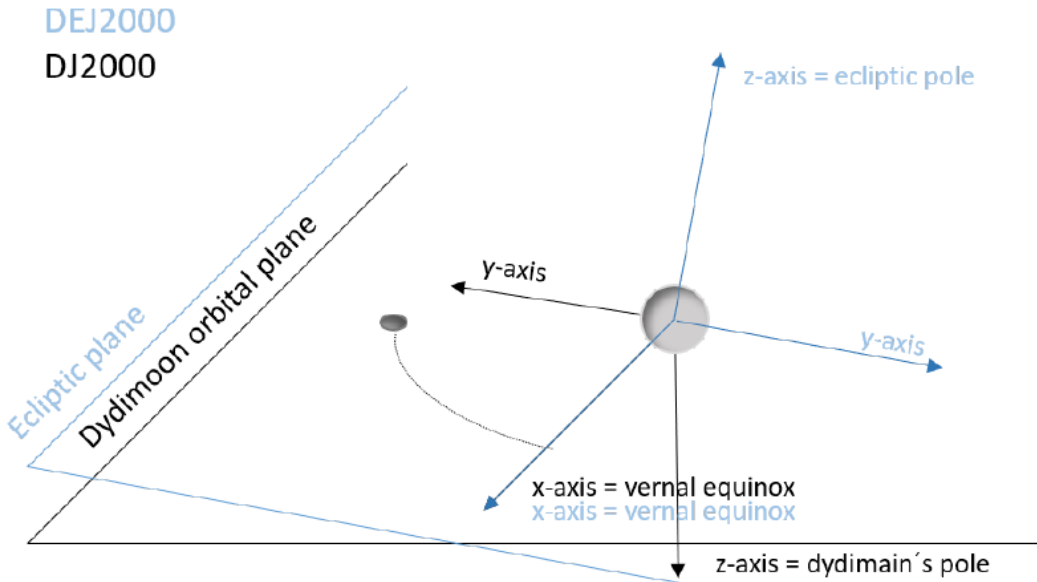


Figure 4-1. Schematic of the inertial frames in use.

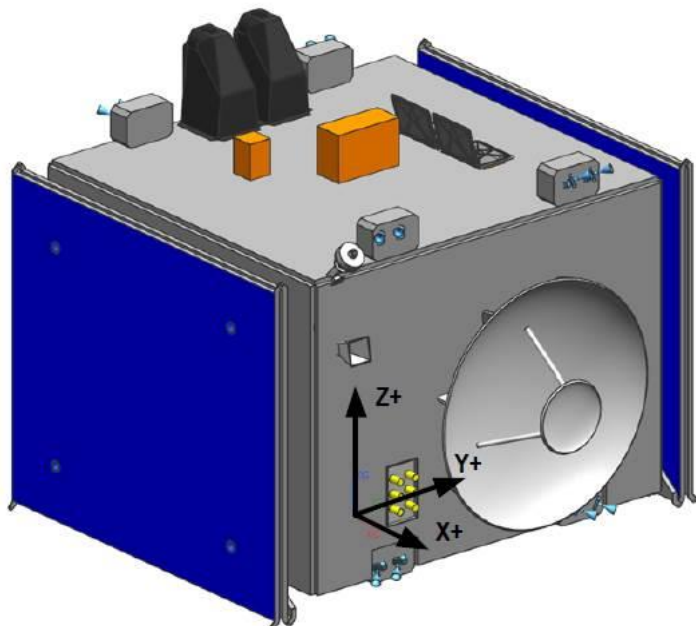


Figure 4-2 HERA SC - Deployer on the +Z face

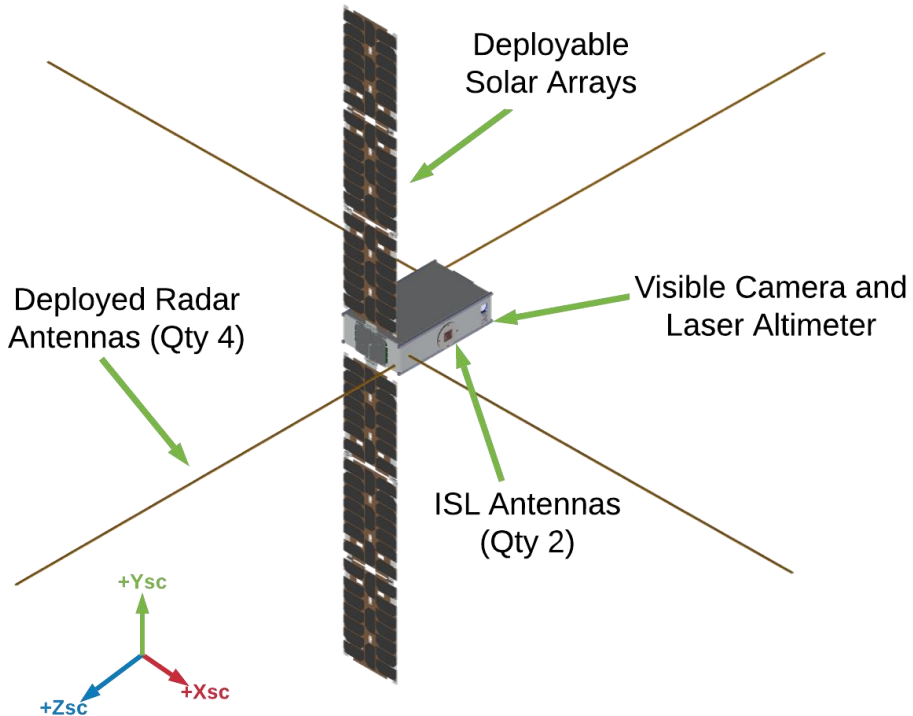


Figure 4-3 Juventas CubeSat reference frame

4.2 CubeSat and Dynamic Parameters

Here below, the parameters used to simulate the Juventas CubeSat are listed.

Table 4-1 Juventas CubeSat considered parameters

	Units	Value
Mass	kg	10
Reflective Surface	m ²	0.464
Reflective Coefficient	-	1.5
Thruster magnitude error	% [3-sigma]	10
Thruster direction error	deg [3-sigma]	3
Isp	s	70
Camera FOV	deg	23.1
Camera Resolution	px	1024x1024

The values used to compute the dynamics around Didymos are listed.

Table 4-2 Didymos considered parameters

	Units	Value	Error (1 sigma)
Didymos mass	kg	5.28 e11	0.2%
Mass ratio	-	0.0093	1%*
			*Assumed knowledge after Hera DCP1
Didymain rotation period	hours	2.26	0.0001
Mean (Didymain) diameter	km	0.780	10%
Mean (Didymoon) diameter	km	0.163	0.018
Distance between Didymoon/Didymain	km	1.18	0.04

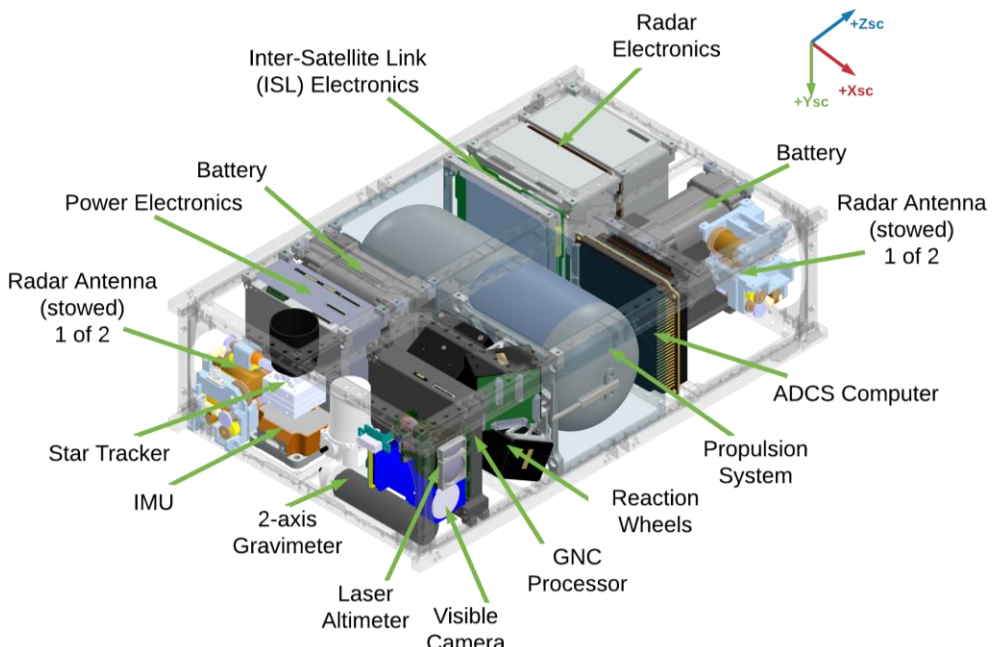


Figure 4-4 Schematic of the Juventas CubeSat

4.3 Mission Profile

Here below, the baseline mission profile is shown. The release and commissioning phase is composed of a single arc of seven days length with the possibility of performing four more seven-day arcs, accounting for a total 35 days duration. Two months are reserved for both observation phases in the nominal scenario. Thus, the total mission duration is 71 days in the nominal case, below the three-month required mission time,(MR-006 in [AD-1] and JUV-OPS-01 in [RD-7]), thus, allowing for extended operations. The contingency case, with the longer commissioning phase lasts 100 days.

Table 4-3 Mission timeline nominal case

<i>Mission Phase</i>	<i>Initial Epoch</i>	<i>Final Epoch</i>	<i>Duration [days]</i>
Release and commissioning Phase	1 st June 2027	8 th June 2027	7*
			*This can extend to a maximum of 35 days for 5 full arcs
Transfer to SSTO	8 th June 2027	11 th June 2027	3
Global Observations Phase	11 th June 2027	11 th July 2027	30
Proximity Observations Phase	11 th July 2027	10 th August 2027	30
Landing Phase	10 th August 2027	10 th August 2027	< 1*
			*A landing rehearsal is included of 1 additional day
Total	1 st June 2027	10 th August 2027	71

4.3.1 Orbit and Pointing Profiles

As the CubeSat is unable to orientate its solar arrays to the Sun without changing the CubeSat attitude, the mission is designed to be as close to the terminator as possible during each phase. This allows to point simultaneously Didymos with the Camera and minimize the inclination of the solar arrays with respect to the sun direction, maximizing the power obtained.

The solar arrays – camera configuration has been selected to optimize the operations during the observation phases. These observations are going to be performed close to the terminator plane due to the SSTO orbit concept that has been proposed and are shown in 5.2.1.

5. Mission Analysis

In this chapter, the mission phases of the Juventas CubeSat are shown. For the simulation of the trajectories of each phase of Juventas a MATLAB simulator will be used. It can compute the required trajectories, maneuvers, and mission related parameters with a 4th-order Runge-Kutta propagator. This was developed during the AIM System Studies. The propagation can be performed either in a inertial reference frame (Ecliptic J2000) centered on Didymain or in a synodic reference frame centered on Didymoon with the x-axis pointing outwards from Didymain's direction, the z-axis with the direction of Didymoon's angular momentum, and the y-axis completing the right-handed orthogonal reference frame. The time-step is chosen as to reduce the propagation error to a negligible order and the following dynamics are considered:

- Didymain, Didymoon, and Sun point mass gravity influence.
- Solar radiation pressure perturbation assuming a constant Section area for the SC and considering eclipses.
- 20th-order non-spherical gravitational potential for Didymain and 4th-order non-spherical potential for Didymoon.
- Didymain's ephemerides are computed from the SPICE kernel provided by ESA.
- Didymoon's ephemerides are computed assuming two body dynamics with Didymain.
- The system's barycenter – Didymain's center-of-mass offset was not considered.

The parameters and values used were summarized in Section 4.2.

The mission phases, in which the operations of the Juventas CubeSat are divided into, are:

- Launch and Commissioning Phase (CP)
- Transfer into Observations Phase (TP)
- Global Observations Phase (GOP)
- Proximity Observations Phase (POP)
- Landing Phase (LP)

5.1 *Launch, Commissioning Orbit, and Transfer Phase (CP and TP)*

Juventas will be released from Hera prior to the Detailed Characterization Phase 2 (DCP-2). Juventas will be released from Hera using a low-velocity deployment pod.

5.1.1 *Release and Commissioning*

The Hera spacecraft will be performing hyperbolic arcs above the minimum distance of 10 kilometers to Didymain. During one of these arcs, Juventas is expected to be released. The deployer is assumed to be placed in the +Z direction of Hera, as per [RD-3]. Due to pointing requirements for Hera, its +Z axis will always point towards Didymain during operations and –X will be always shadowed. This geometry constraints the possible release directions of Juventas. Furthermore, it is required that Juventas is not released along the velocity vector of Hera.

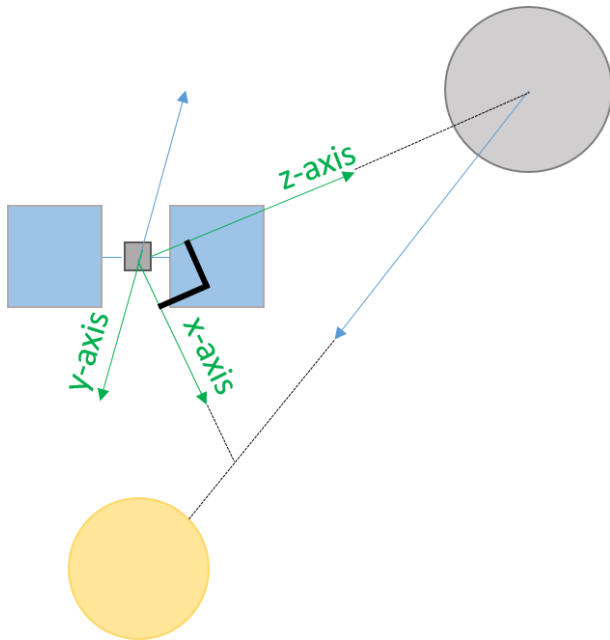


Figure 5-1. HERA's nominal attitude schematic.

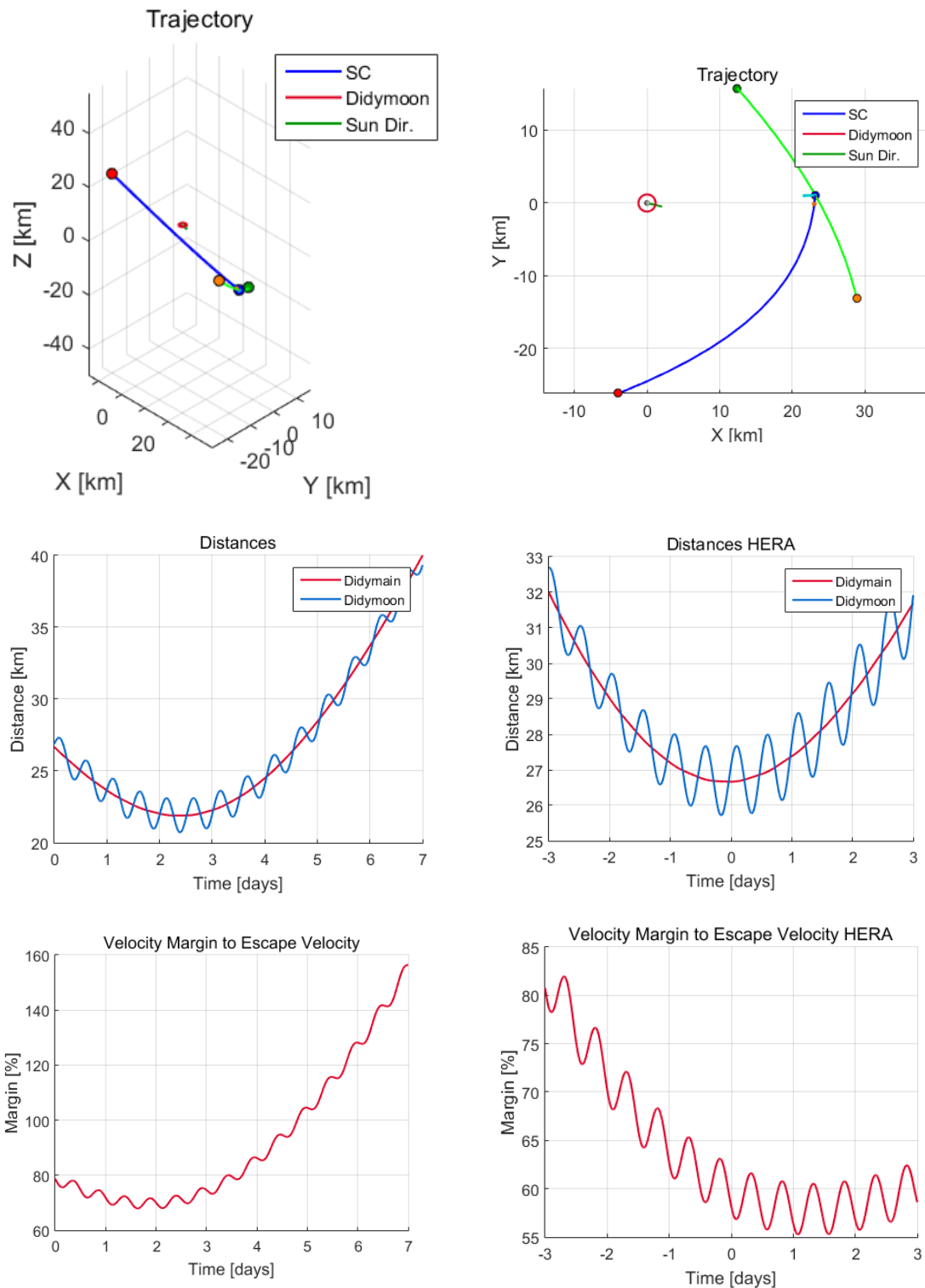
After the release, the CubeSat must be inserted in a safe trajectory with minimum four days without operations, to allow checks and prepare to command the CubeSat. This trajectory is designed to be passively safe, not to require any active operations to guarantee its safety during its execution. The duration is extended to seven days to account for contingencies.

Besides, it must be ensured that HERA release trajectory is also passively safe within ± 3 days since the release. This approach achieves not putting Hera in risk during the CubeSat release. Finally, Hera's hyperbolic arcs must also be in phase angles below 90° to optimize the performance of the Image Processing algorithms.

Considering all the criteria, the trajectories are generated travelling between waypoints with a fixed duration. To select the waypoints, the sun direction is used to reference the points to Didymos. This way, it is possible to choose points in the terminator plane at every epoch.

Once the release arc has been defined, the release point is known, and it is possible to know the Hera attitude at this point. Thus, projecting the initial velocity of the previously defined arc into the $-Y$ Hera direction, the deployer velocity mechanism is obtained. The remaining component of the velocity should be provided by Hera spacecraft velocity; therefore, Hera trajectory is already defined.

The **release velocity** to be provided by the **deployer** mechanism is found to be **2 cm/s** for the trajectory shown in Figure 5-2. Due to the intrinsically safe design of the commissioning phase trajectory, the accuracy of the release mechanism is not observed to have a significant impact on the design,



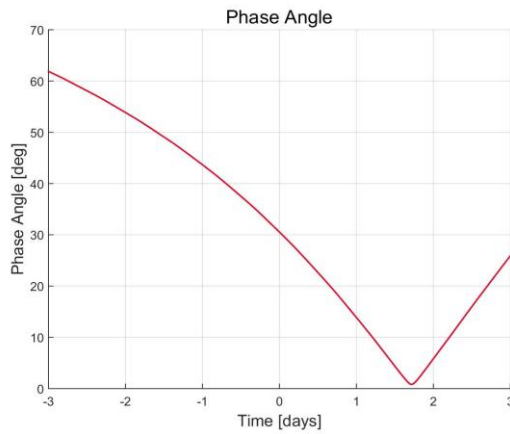


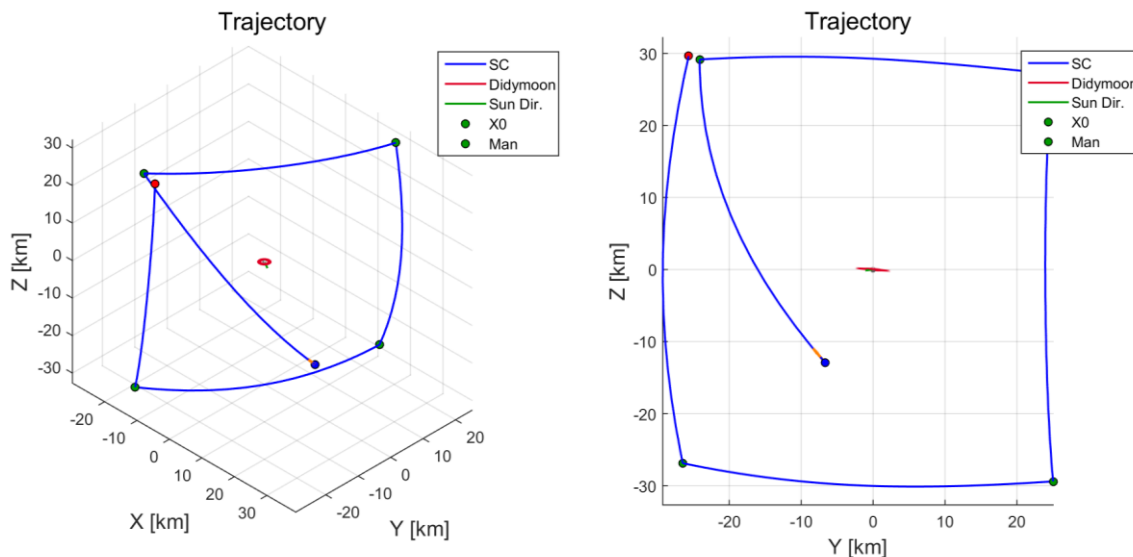
Figure 5-2 Juventas and HERA – Release Orbit – Trajectory, distance, velocity margin, and phase angle

5.1.2 Training Orbit

If, for some reason, the operations team does not feel confident enough to inject the CubeSat into the operational orbit, the following approach is proposed:

- Hera's Early-Characterization Phase (ECP) like trajectories.
 - Four hyperbolic arcs at 30 km minimum distance to Didymoon, distributed in a square shape.
 - Duration of all arcs is seven days, with a maximum of 35 days.
 - Two polar and two vertical arcs in the terminator plane to allow simultaneous asteroid pointing and Sun pointing to the solar arrays.

This approach is meant to give injection possibilities every seven days to account for contingencies.



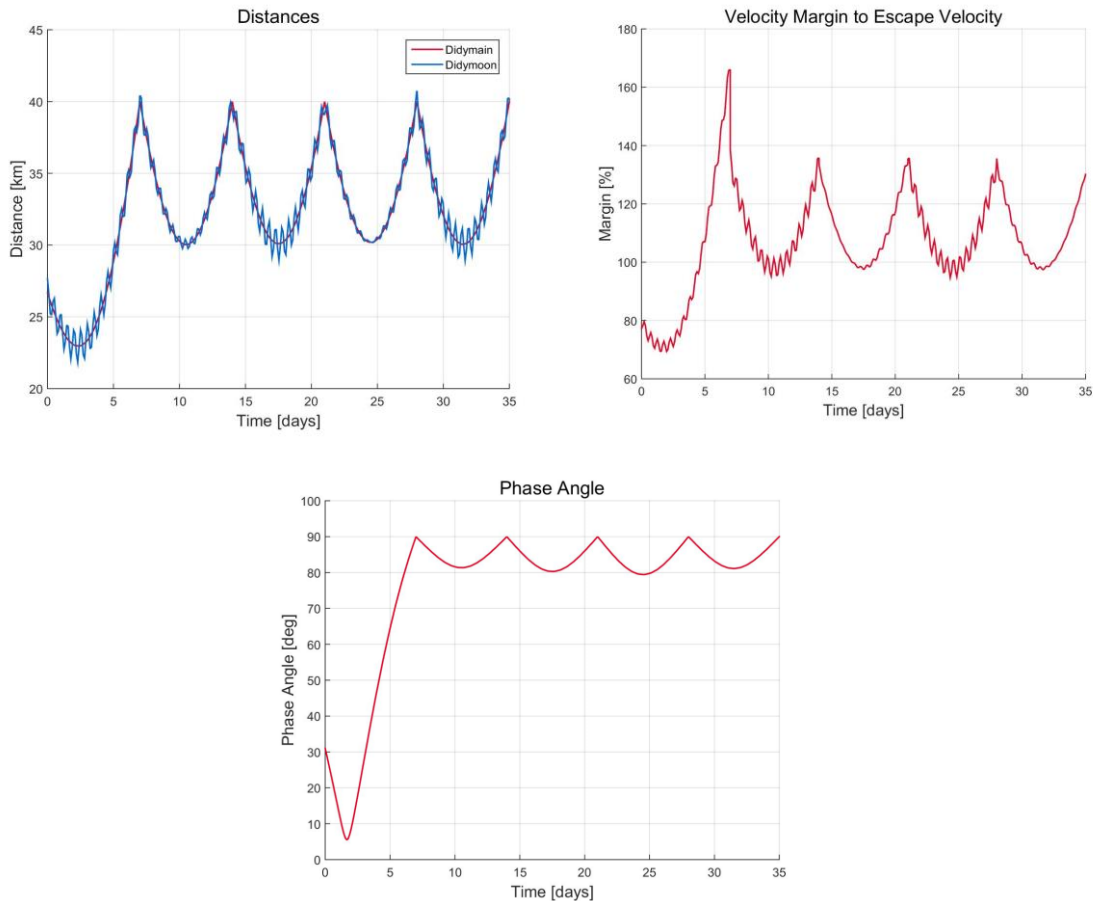


Figure 5-3 Juventas – Release and Training Orbit – Trajectory, distance, velocity margin, and phase angle

5.1.3 Transfer Phase

Finally, once the commissioning phase is over, Juventas will be injected into an SSTO. In order to perform this transfer with safety, the same constraints regarding the hyperbolic transfers used for the design of the previous stages is used.

- Velocity always 40% above the local escape velocity. In case of failure at insertion, the CubeSat is in a collision free trajectory and the control of the CubeSat could be recovered several days after.
- Arc length as a multiple of Earth days to ease operations. In this case the arc is designed to last 3 days.
- Critical operations are planned to minimize dispersion at the SSTO insertion. Making a correction one day before the injection can significantly reduce the dispersion at the insertion point. This reduction leads to improved conditions at the insertion
- Velocity arrival of transfer arc is tangent to SSTO trajectory. Thus, delta-V required is minimized and the thruster errors associated to the maneuver are also minimized. This allows a wider range of thruster errors to insert safely into the SSTO as it has been analyzed in [RD-4].

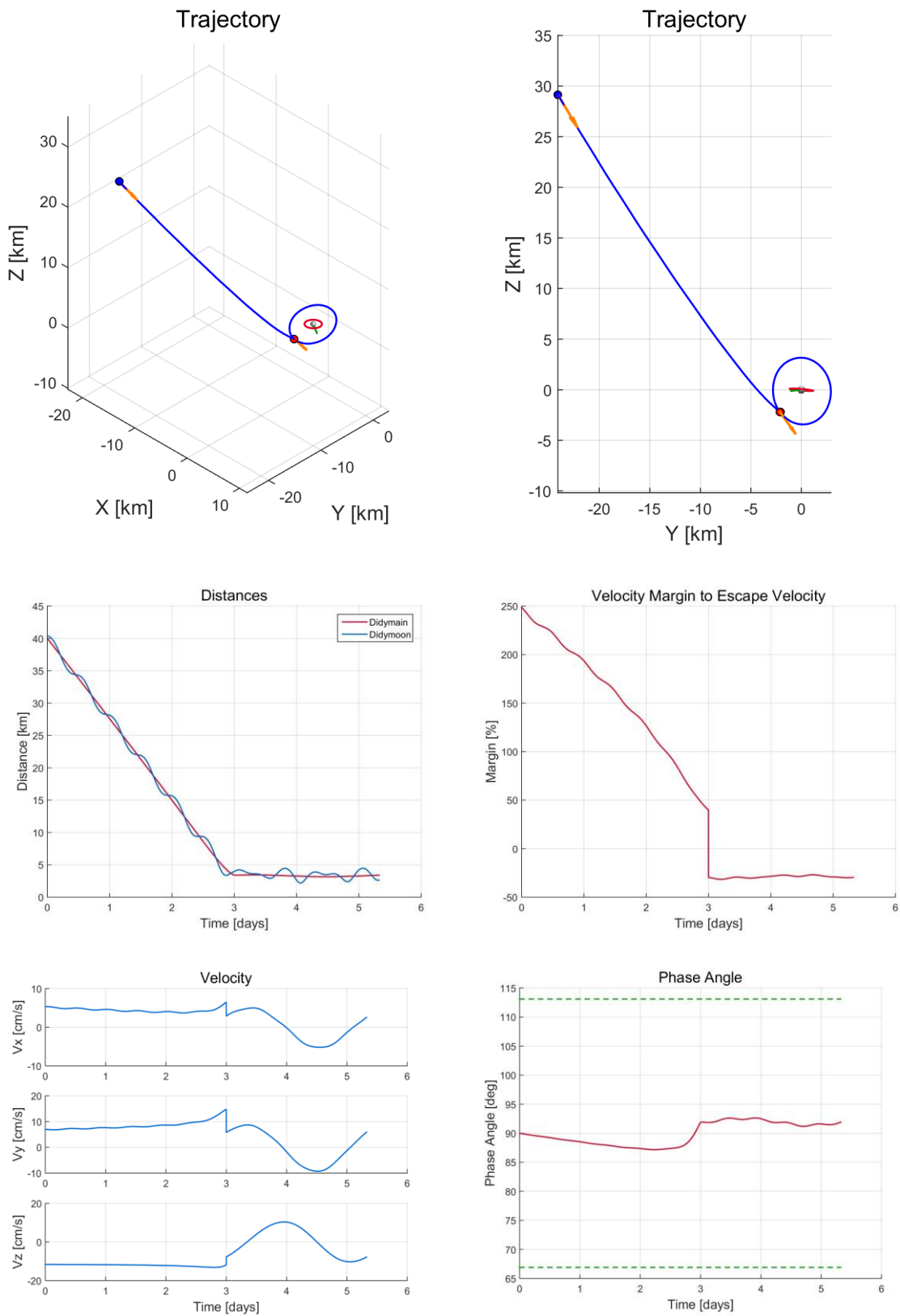


Figure 5-4 Juventas – Transfer to SSTO – Trajectory, distance, velocity margin, velocity, and phase angle

5.2 Observations Phases (GOP and POP)

5.2.1 Proposed Orbits

The proposed baseline for the Observations Phase of the Juventas CubeSat are self-stabilized terminator orbits (SSTO). The SSTOs, also called photo-gravitational orbits, has been studied for a large number of missions as in [RD-5] and [RD-6]. The interest of these orbits lies in the scientific return obtained when orbiting them and the reduced number operations required.

The SSTOs arise from the existence of an equilibrium point that corresponds to a low-eccentricity orbit, offset from the center of the point mass along the direction x and perpendicular to this same direction, where the SRP perturbation is equal to the x-component of the gravitational force of the central body. A depiction of these orbits where their most important parameters are shown, can be seen in Figure 5-5.

Thus, this type of orbits is selected as the baseline on which perform the surface characterization of the Didymos system.

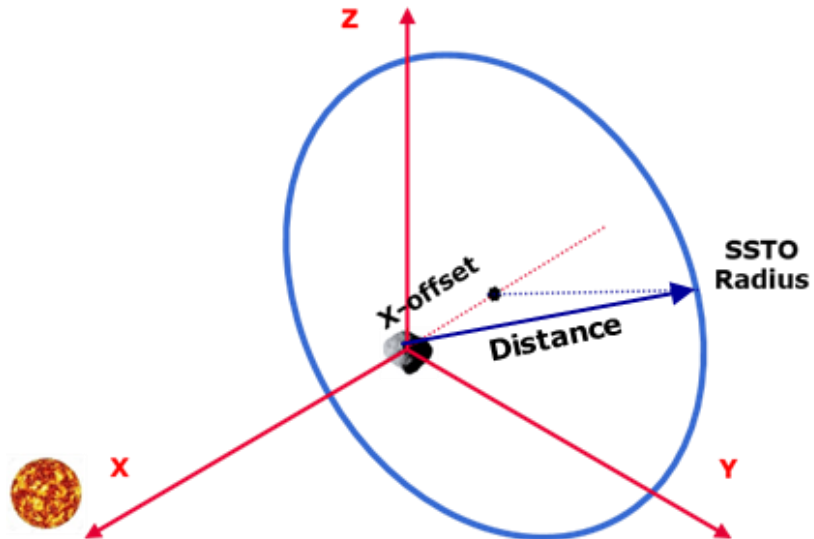


Figure 5-5 Schematic of an SSTO

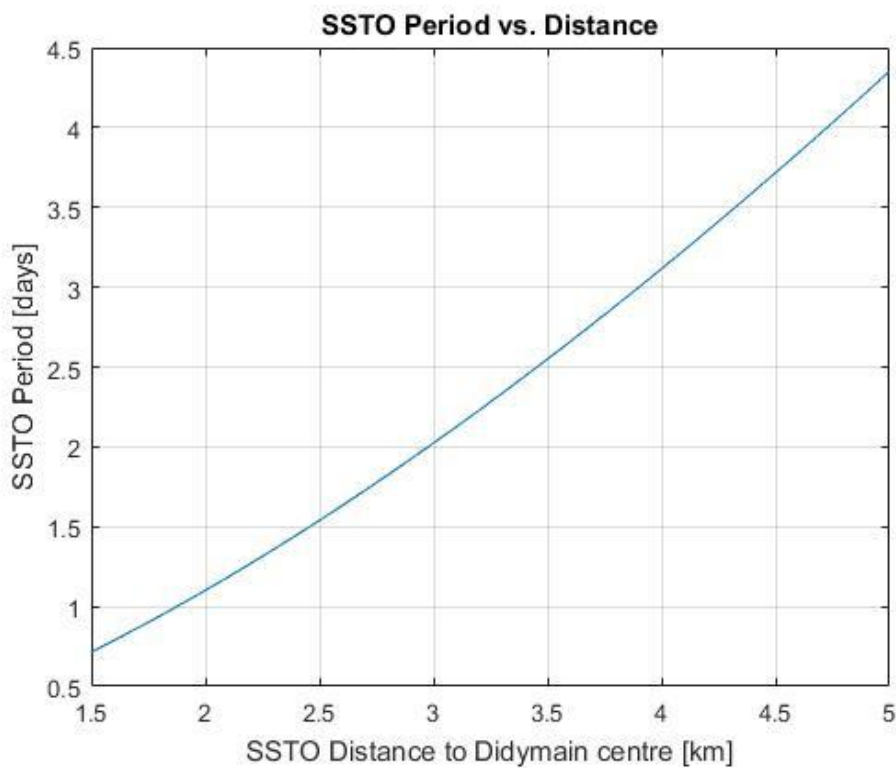


Figure 5-6 SSTO Period as a function of the distance to Didymain

5.2.2 Coverage Analysis

In order to properly select the baseline orbits for the observation phases of Juventas, one key aspect is the quality of the surface reconstruction. This task is performed by the on-board radar.

5.2.2.1 Assumptions

The ground track is coincident with the sub-satellite points due to the character of radar measurements. Both, Didymoon and Didymain are spheres of constant radius.

Eccentricity of SSTO orbits is neglected and are assumed as circular orbits.

The **swath** is defined to cover a **5-meter (TBC)** resolution at a **distance of 5 km** (3.5 arcmin).

5.2.2.2 Occultation Conditions

The following image represents the visibility conditions to allow a measurement of the surface of Didymoon.

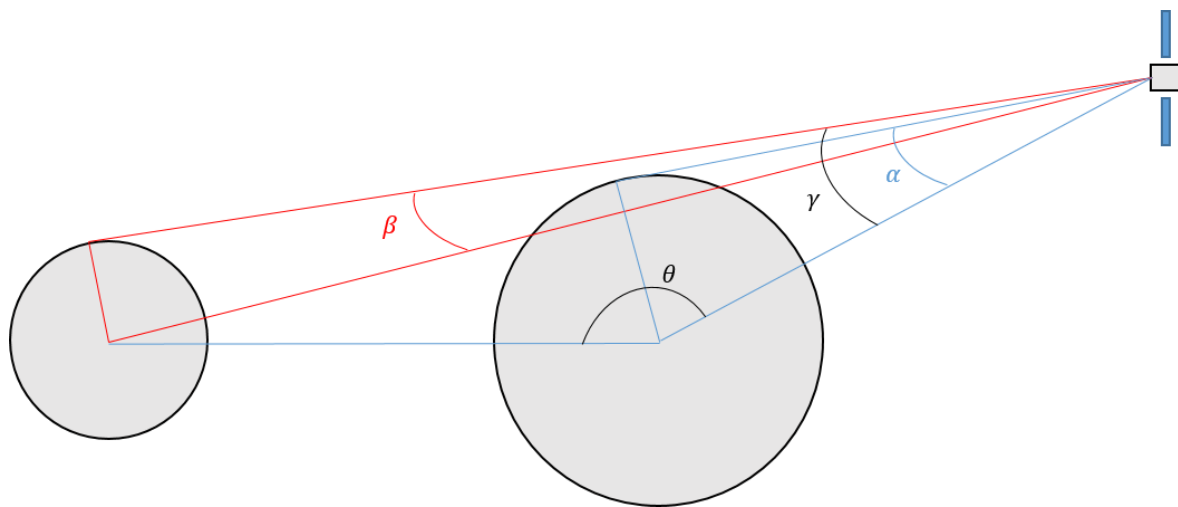


Figure 5-7. Schematic of the visibility conditions of the Juventas CubeSat.

Didymoon's occultation conditions are the following:

$$\begin{aligned}\gamma &< \alpha + \beta \\ \theta &> 90^\circ\end{aligned}$$

And the same approach is used for Didymain.

5.2.2.3 Resonant Orbits

The ground track of resonant orbit causes periodic ground track shapes. Thus, it is convenient to avoid these resonances to achieve the maximum coverage, filling the gaps in between consecutive ground tracks.

5.2.2.3.1 Didymoon Resonance

Here, the $n \times m$ resonant SSTOs for Didymoon are shown. Where m and n , are integers defined as

$$n T_{SSTO} = m T_{didymoon}$$

Thus, the SSTO Didymain distance is obtained from the resonant periods. The below table shows the SSTO Didymain distance in km as a function of m and n .

Table 5-1. SSTO-Didymain for Didymoon resonant periods (in orange are selected orbits for the coverage analysis).

m	n		
	1	2	3
1	1,18	0,74	0,57
2	1,87	1,18	0,90
3	2,45	1,54	1,18
4	2,96	1,87	1,42
5	3,44	2,17	1,65
6	3,88	2,45	1,87
7	4,30	2,71	2,07
8	4,71	2,96	2,26
9	5,09	3,21	2,45

10	5,46	3,44	2,62
11	5,82	3,67	2,80
12	6,17	3,88	2,96
13	6,50	4,10	3,13
14	6,83	4,30	3,28
15	7,15	4,51	3,44
16	7,47	4,71	3,59
17	7,78	4,90	3,74
18	8,08	5,09	3,88
19	8,38	5,28	4,03
20	8,67	5,46	4,17
21	8,95	5,64	4,30
22	9,24	5,82	4,44
23	9,51	5,99	4,57
24	9,79	6,17	4,71
25	10,06	6,34	4,83
26	10,32	6,50	4,96
27	10,59	6,67	5,09
28	10,85	6,83	5,21
29	11,10	6,99	5,34
30	11,36	7,15	5,46

5.2.2.3.2 Didymain Resonance

Here, the $n \times m$ resonant orbits for Didymain are shown. Where m and n are defined as

$$n T_{SSTO} = m T_{didymain}$$

Thus, the SSTO Didymain distance is obtained from the resonant periods. The below table shows the SSTO Didymain distance in km as a function of m and n.

Table 5-2. SSTO-Didymain for Didymain resonant periods (in orange, selected orbits for the coverage analysis).

m	n			
	1	2	3	4
30	3,75	2,36	1,80	1,49
31	3,83	2,41	1,84	1,52
32	3,91	2,46	1,88	1,55
33	3,99	2,52	1,92	1,58
34	4,07	2,57	1,96	1,62

35	4,15	2,62	2,00	1,65
36	4,23	2,67	2,03	1,68
37	4,31	2,72	2,07	1,71
38	4,39	2,76	2,11	1,74
39	4,46	2,81	2,15	1,77
40	4,54	2,86	2,18	1,80
41	4,62	2,91	2,22	1,83
42	4,69	2,95	2,25	1,86
43	4,76	3,00	2,29	1,89
44	4,84	3,05	2,33	1,92
45	4,91	3,09	2,36	1,95
46	4,98	3,14	2,40	1,98
47	5,06	3,18	2,43	2,01
48	5,13	3,23	2,46	2,03
49	5,20	3,27	2,50	2,06
50	5,27	3,32	2,53	2,09
51	5,34	3,36	2,57	2,12
52	5,41	3,41	2,60	2,15
53	5,48	3,45	2,63	2,17
54	5,55	3,49	2,67	2,20
55	5,61	3,54	2,70	2,23
56	5,68	3,58	2,73	2,25
57	5,75	3,62	2,76	2,28
58	5,82	3,66	2,80	2,31
59	5,88	3,71	2,83	2,33
60	5,95	3,75	2,86	2,36
61	6,02	3,79	2,89	2,39
62	6,08	3,83	2,92	2,41
63	6,15	3,87	2,95	2,44

64	6,21	3,91	2,99	2,46
65	6,28	3,95	3,02	2,49
66	6,34	3,99	3,05	2,52
67	6,40	4,03	3,08	2,54
68	6,47	4,07	3,11	2,57
69	6,53	4,11	3,14	2,59
70	6,59	4,15	3,17	2,62
71	6,66	4,19	3,20	2,64
72	6,72	4,23	3,23	2,67
73	6,78	4,27	3,26	2,69
74	6,84	4,31	3,29	2,72
75	6,90	4,35	3,32	2,74
76	6,97	4,39	3,35	2,76
77	7,03	4,43	3,38	2,79
78	7,09	4,46	3,41	2,81
79	7,15	4,50	3,44	2,84
80	7,21	4,54	3,46	2,86

As Didymain's period is very fast, these resonances do not have a high influence in the Didymain ground track.

5.2.2.4 *Didymoon Coverage*

Here below, the coverage analysis of the Juventas CubeSat on Didymoon is depicted.

5.2.2.4.1 **Didymain shadow**

As the system is supposed to be tidally locked, the same zone of Didymoon is always pointing towards Didymain, and due to the geometry of the SSTO and Didymain position, a shadow appears in the Didymoon ground track.

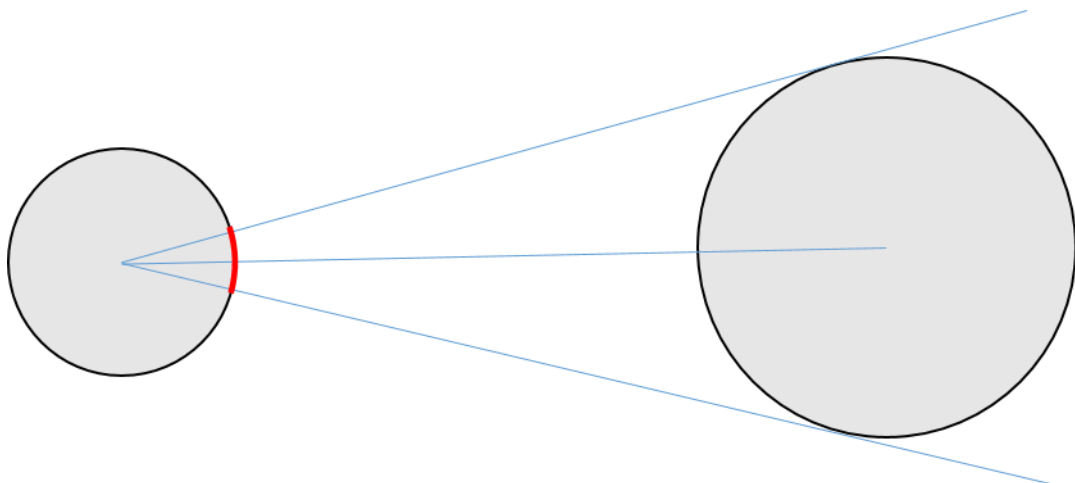


Figure 5-8. Didymain shadow on Didymoon's ground track.

The figure above depicts the forbidden area of Didymoon in red. This shadow can be computed theoretically as the percentage of the spherical cap area with respect to the Didymoon total area. For Didymain, this area approximately represents a 3% of the total surface.

The ground track of a 1.5 km SSTO is shown below. The shadow is clearly seen in the center of the image. The other two unobserved locations are not tracked due to the selection of the SSTO as the baseline orbit and the obliquity of the polar axis of Didymoon. These areas can be observed if different SSTO heights are used.

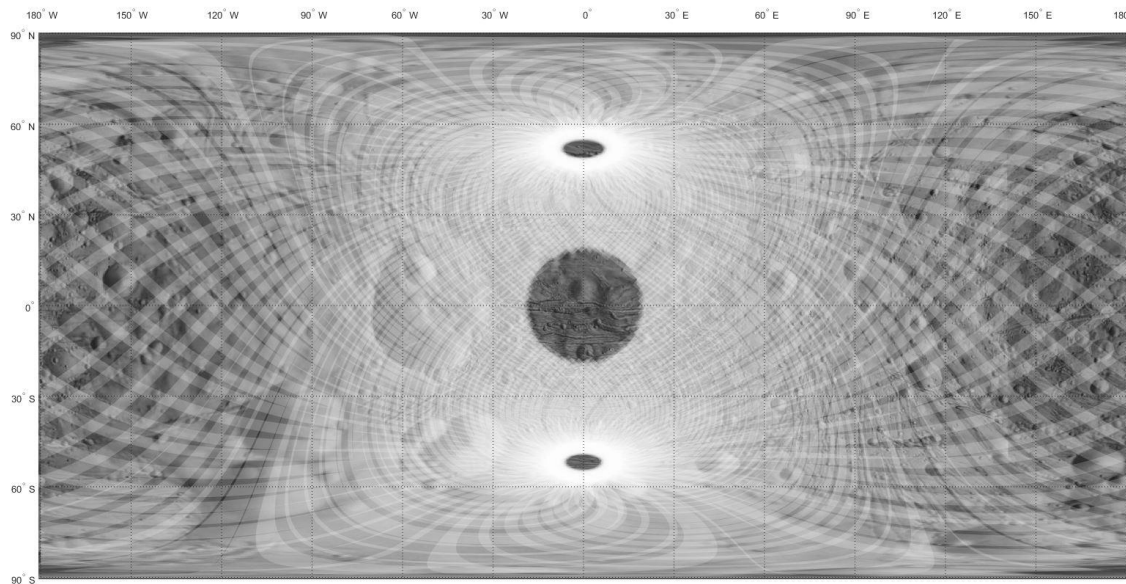


Figure 5-9. Didymoon ground track for a 1.5 km SSTO for 60 days.

5.2.2.4.2 Coverage analysis for a single operational orbit

The coverage percentage for a mesh of different distances hold for different durations are summarised in the table below.

Table 5-3. Didymoon coverage for a mesh of radius and durations (in orange, two resonant orbits).

	SSTO Distance [km]
--	--------------------

Duration [days]	1.5	2	2.5	3	3.5	4	4.5	5	5.5	6	6.5	7	7.5	8
5	18	20	16	22	17	23	20	21	17	19	22	25	27	30
10	34	34	34	38	32	36	31	36	33	38	25	41	34	41
15	46	48	47	56	46	49	37	53	47	43	26	48	41	54
20	55	58	50	64	58	63	45	60	61	48	28	50	53	66
25	60	67	54	70	69	70	51	66	72	51	29	53	58	74
30	66	71	57	76	77	80	57	71	81	55	32	55	65	84
35	71	74	59	84	83	84	63	77	87	59	33	57	71	86
40	75	77	62	90	87	85	68	82	91	62	35	60	75	91
45	78	80	65	93	87	87	72	86	93	65	36	61	82	92
50	80	82	67	93	87	88	77	90	94	69	37	63	86	94
55	82	84	70	94	87	89	80	92	94	73	39	65	88	95
60	83	86	73	94	87	90	83	94	94	76	40	67	93	95
65	85	88	74	94	87	91	86	95	94	78	41	69	94	95
70	86	89	77	94	88	92	88	95	95	81	43	71	95	95
75	87	91	79	95	88	92	91	96	95	83	44	73	96	95
80	88	92	80	95	88	93	93	96	95	85	46	75	96	96
85	88	93	82	95	88	93	94	96	95	87	47	76	96	96
90	89	94	84	95	88	94	95	96	95	89	48	79	96	96

The coverage is significantly lower when a resonant orbit is flight as it is shown for the 6.5 and 7 km orbits. An example of a 6.5 km resonant SSTO ground track is shown below.

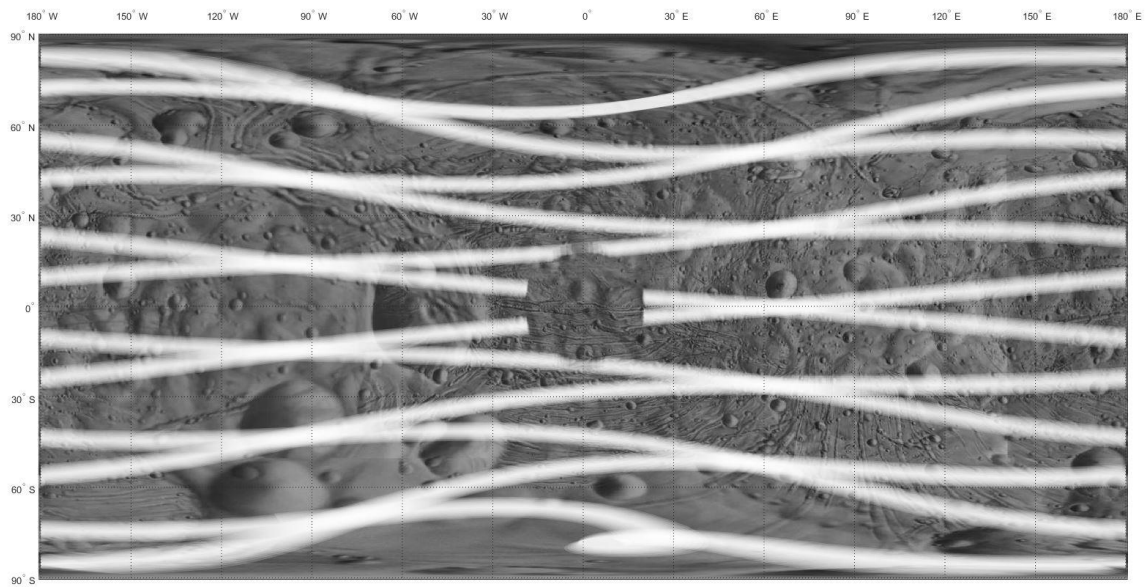


Figure 5-10. Didymoon ground track of a resonant SSTO.

An example of a 5 km non-resonant SSTO ground track is shown below.

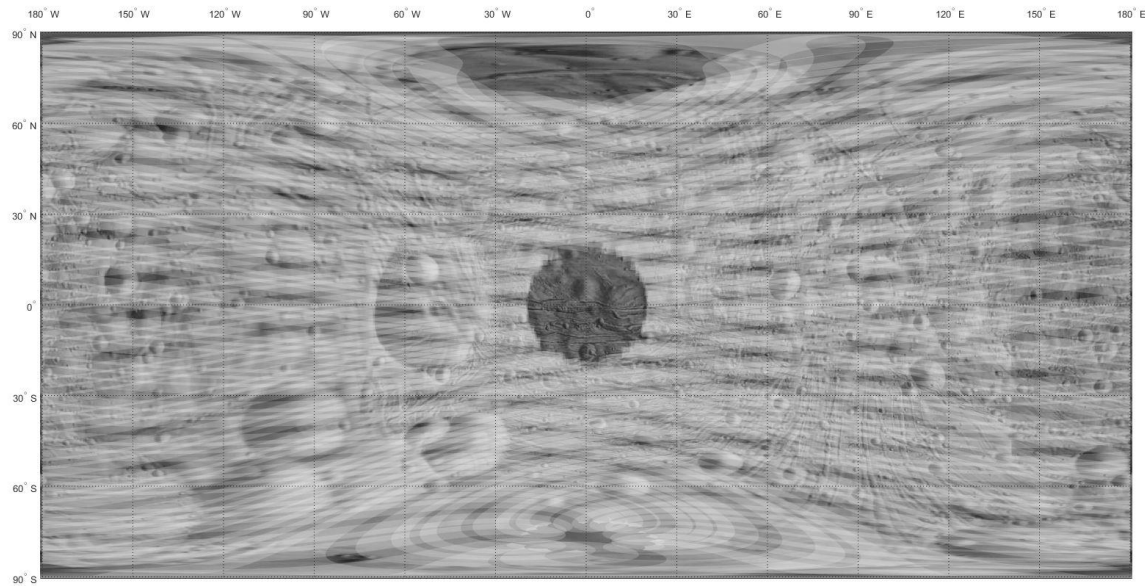


Figure 5-11. Didymoon ground track of a non-resonant SSTO.

The summary of coverage of Didymoon for each of the SSTO orbit distances is shown in the plot below.

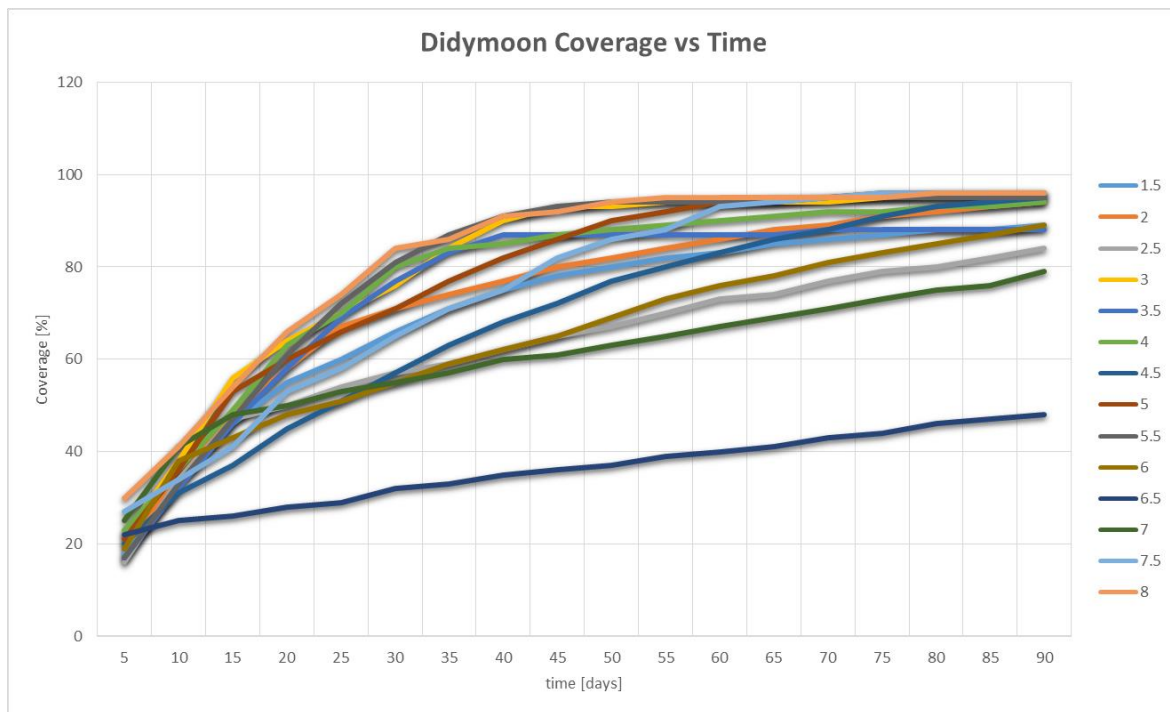


Figure 5-12 Didymoon coverage vs time

5.2.2.5 *Didymain Coverage*

5.2.2.5.1 SSTO Didymain coverage limit

The figure below depicts the unobservable zones of Didymain when an SSTO is used.

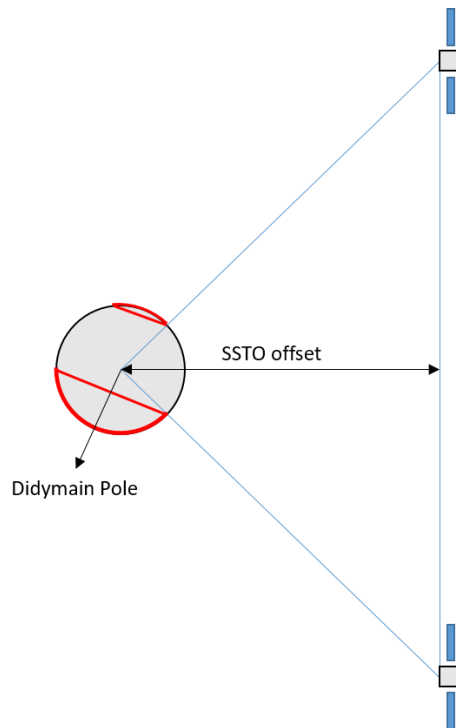


Figure 5-13. Schematic of the unobservability of the poles of Didymos

The red lines represent the forbidden zones of Didymos for a given SSTO. As Didymos pole is slightly tilted with respect to the SSTO plane, the visibility is not going to be equal in both poles. A ground track example for a 7 km SSTO and a duration of 60 days is shown below.

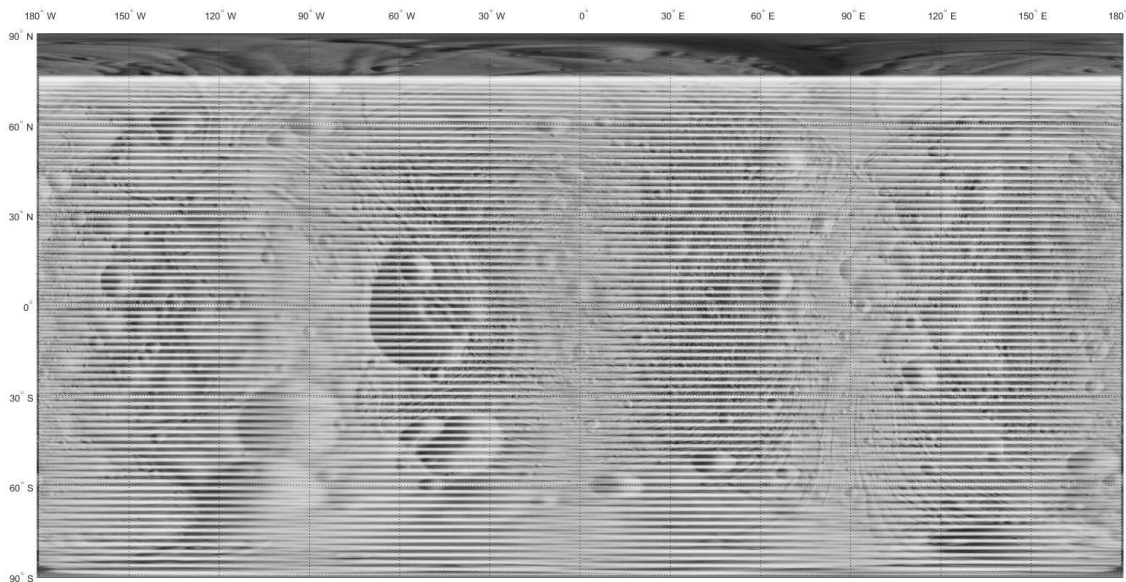


Figure 5-14. Didymos ground track of a 7 km SSTO for 60 days.

As it is expected the only invisible zones are near the poles while in the North Pole the phenomena is highly marked. This phenomenon is higher in the North Pole as the higher the SSTO offset is. For a SSTO of 3km the offset is still low, and the poles are similarly covered.

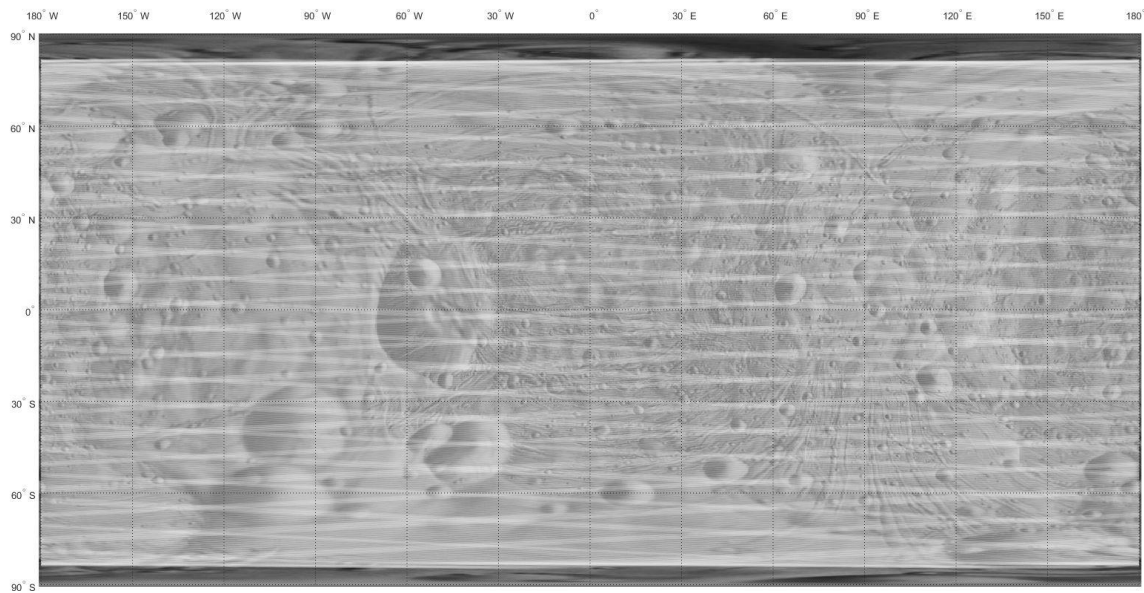


Figure 5-15. Didymos ground track of a 3 km SSTO for 60 days

As it can be observed, the geometries of all ground tracks are nearly perpendicular to the Didymos rotation axis. This is due to the fast rotation of Didymos body w.r.t. the movement in the SSTO orbit.

5.2.2.5.2 Coverage analysis for a single operational orbit

The coverage percentage for a mesh of different distances hold for different durations are summarised in the table below.

Table 5-4. Didymos coverage for a mesh of radius and durations.

Duration [days]	SSTO Distance [km]								
	1.5	2	2.5	3	3.5	4	4.5	5	
5	22	24	22	25	22	25	26	26	
10	41	41	36	39	42	41	45	45	
15	57	57	46	55	58	55	59	63	
20	71	64	56	66	72	70	74	76	
25	82	71	66	78	83	79	84	78	
30	90	77	75	86	92	89	92	80	
35	93	83	82	92	97	94	97	83	
40	95	88	87	97	99	98	100	86	
45	97	92	93	99	99	100	100	89	
50	98	96	97	100	99	100	100	92	
55	99	98	99	100	99	100	100	94	

60	100	99	100	100	99	100	100	96
65	100	100	100	100	100	100	100	98
70	100	100	100	100	100	100	100	99
75	100	100	100	100	100	100	100	100
80	100	100	100	100	100	100	100	100
85	100	100	100	100	100	100	100	100
90	100	100	100	100	100	100	100	100

Despite a maximum limit has been depicted before, the rotation of the SSTO makes the CubeSat achieve the whole coverage for long enough observation times (above 60 days).

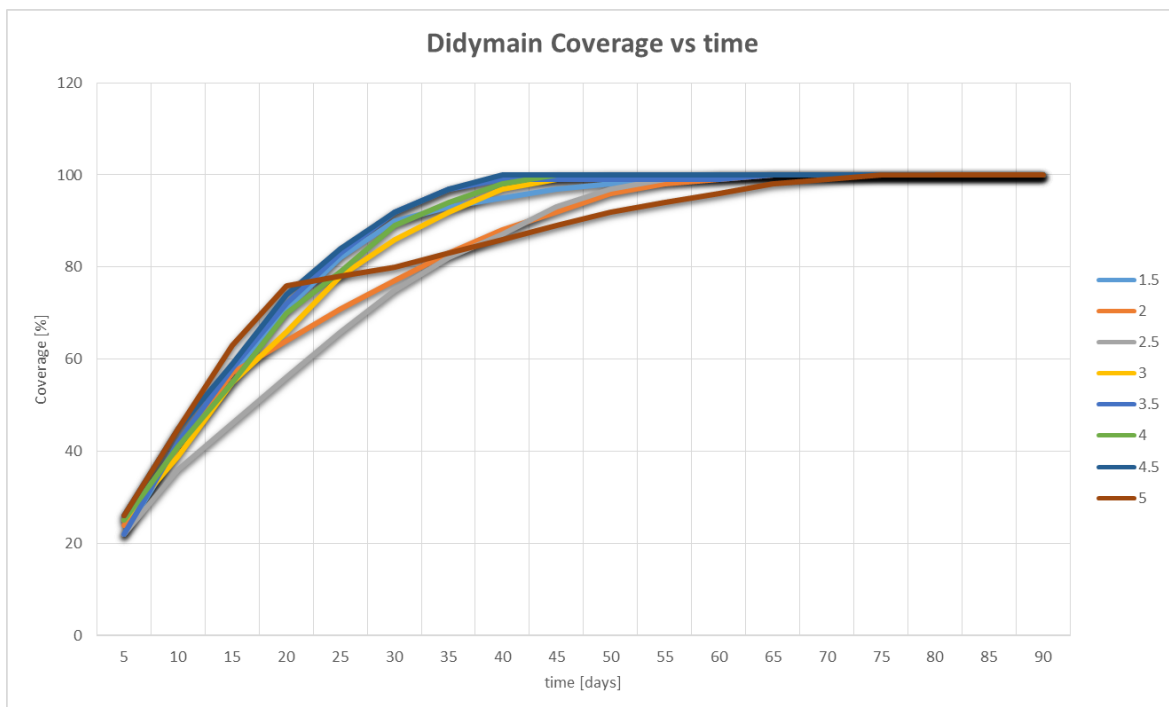


Figure 5-16 Didymain coverage vs time

5.2.2.6 Conclusions

Didymoon and Didymain 70 % coverage can be guaranteed for 60 days of observations with alternative pointing. Longer observation operations would lead to an increased coverage for both bodies. The single orbit option reduces the operational complexity compared to using multiple orbits for observation. However, using the multiple orbits option, the same areas can be observed under different conditions/geometries.

Resonant orbits must be avoided to maximize the coverage.

5.2.3 Global Observations Phase (GOP)

The selected baseline for the global observations phase of the Juventas CubeSat is a 3.30 km distance SSTO.

Figure 5-17 shows the SSTO in two different reference frames, Didymos synodic and Ecliptic J2000. The SSTO is frozen in the synodic reference frame, while in Ecliptic, the plane orientation follows the wander in the Sun direction.

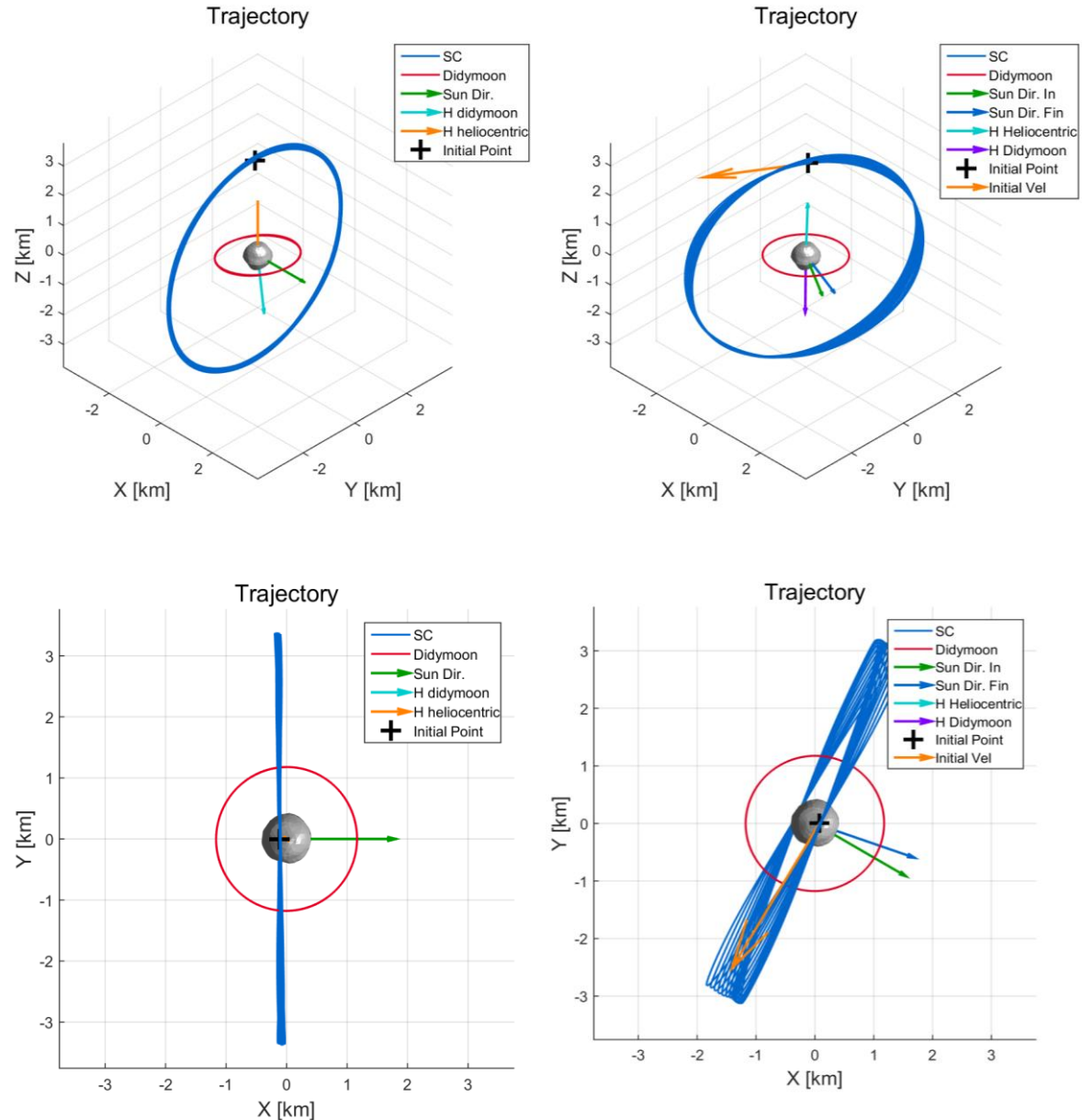


Figure 5-17. 3.3 km SSTO in Synodic (left) and Ecliptic (right).

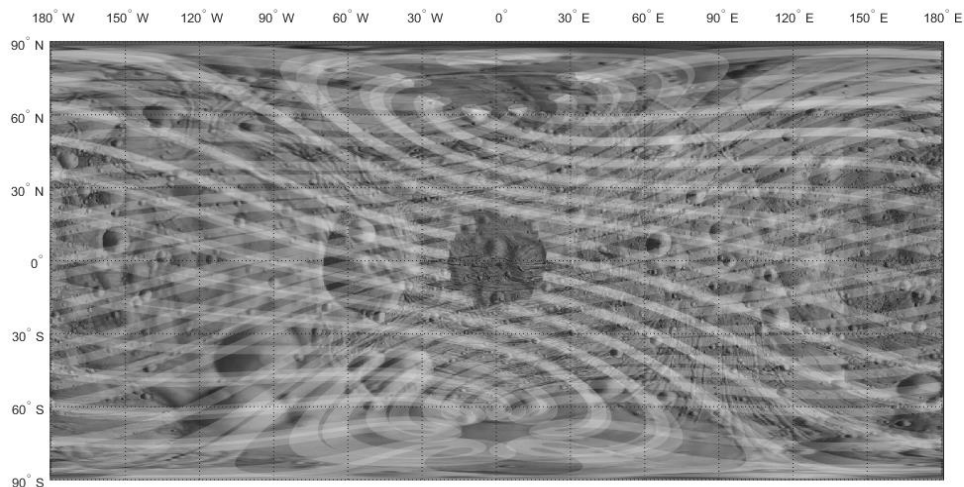


Figure 5-18 Didymoon ground track during the global observations phase SSTO 3.3 km

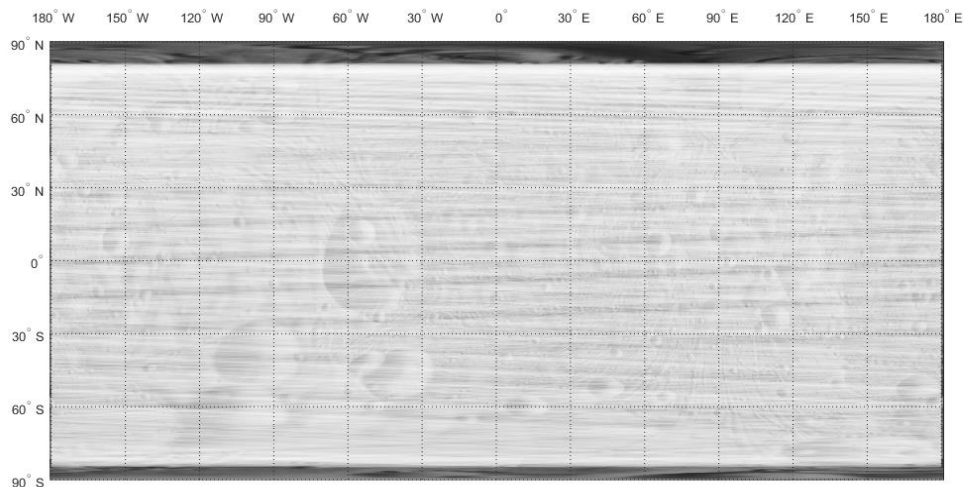


Figure 5-19 Didymain ground track during the global observations phase SSTO 3.3 km

5.2.4 Proximity Observations Phase (POP)

The selected baseline for the Proximity Operations Phase is a 2.00 km distance SSTO. Figure 5-20 shows the SSTO in two different reference frames, Didymos synodic and Ecliptic J2000, where the same effect as in Figure 5-17 is observed.

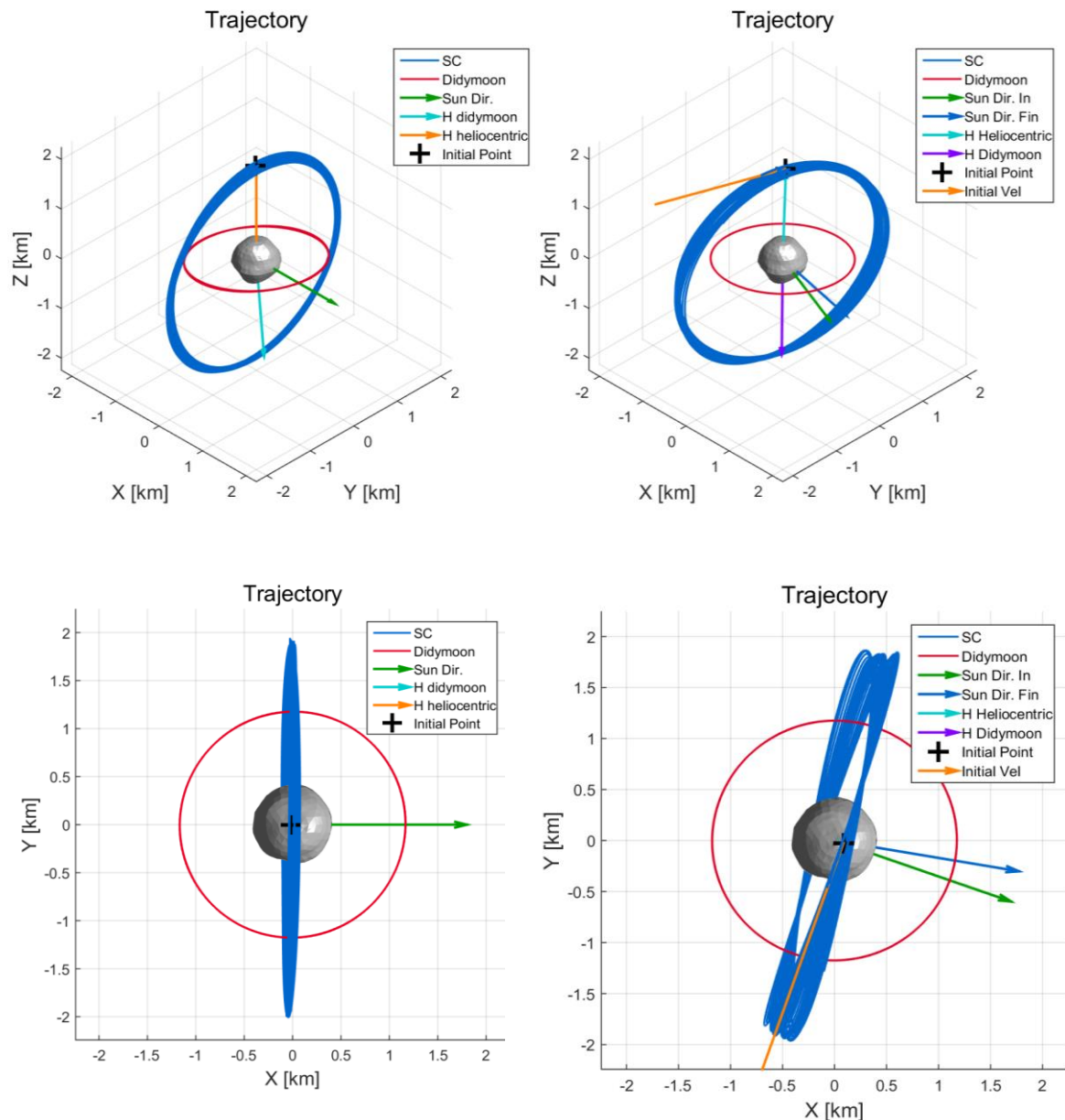


Figure 5-20. 2 km SSTO in Synodic (left) and Ecliptic (right).

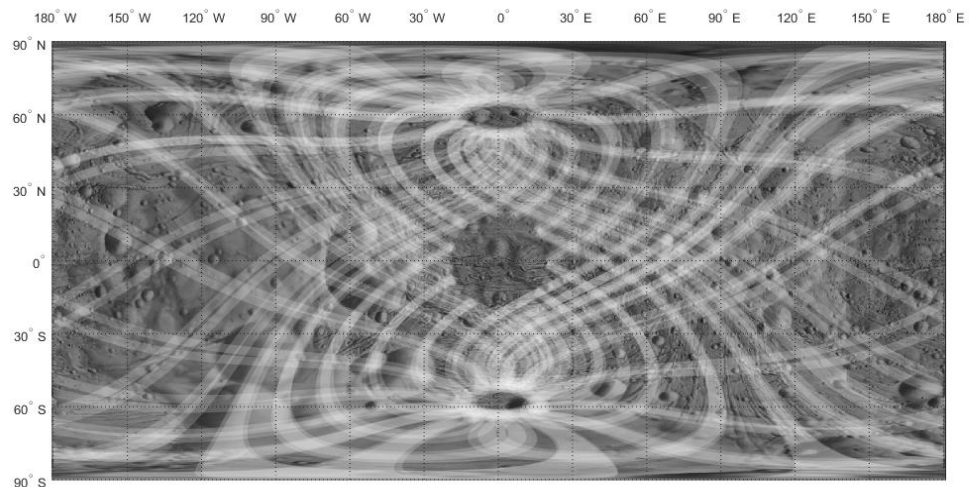


Figure 5-21 Didymoon ground track during the global observations phase SSTO 3.3 km

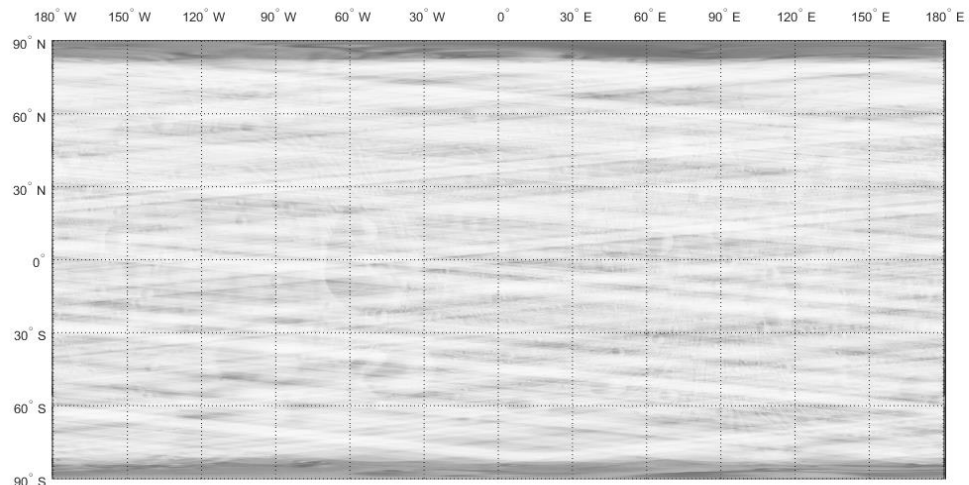


Figure 5-22 Didymain ground track during the global observations phase SSTO 3.3 km

5.2.5 Complete Coverage during the Observations Phases

Table 5-5 Surface coverage during the Observations Phases

	<i>Didymoon Coverage [%]</i>	<i>Didymain Coverage [%]</i>
Global Observations Phase	71.89	99.2
Proximity Observations Phase	63.5	99.29
Total Observations Phases	88	99.4

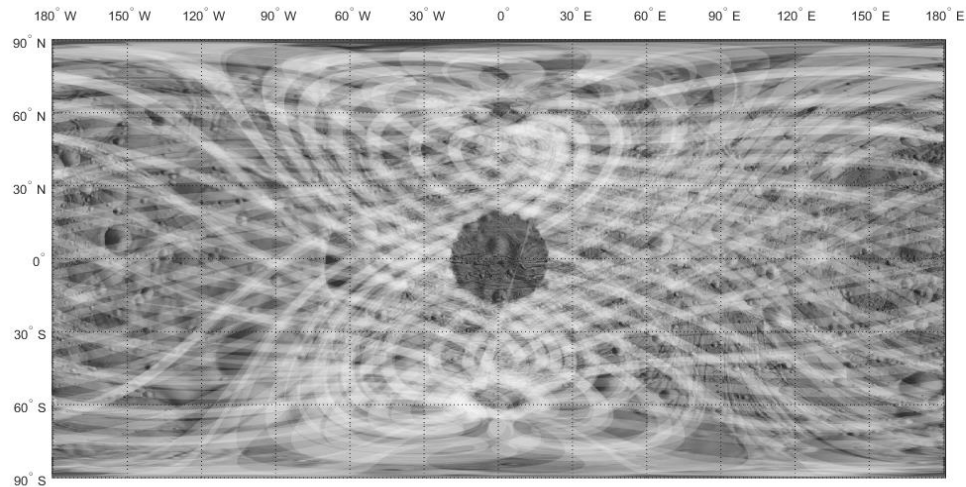


Figure 5-23 Didymoon ground track during the global observations phase SSTO 3.3 km

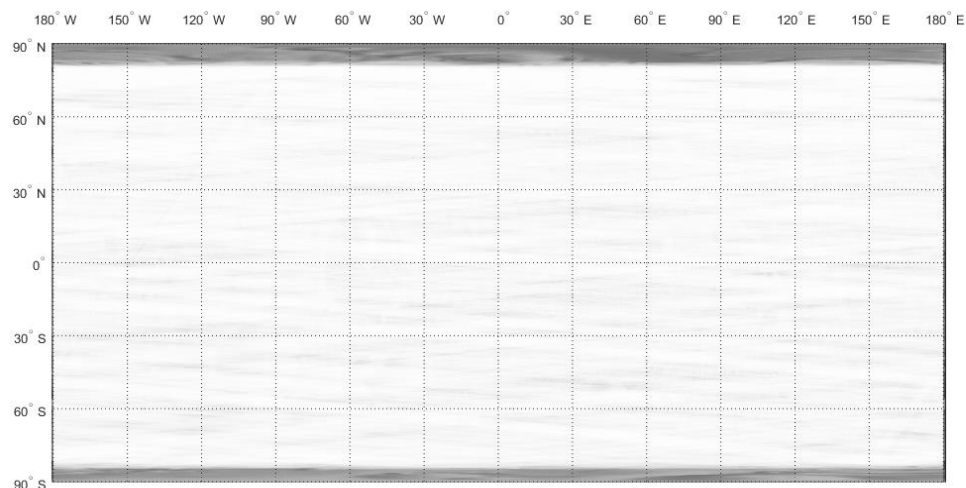


Figure 5-24 Didymain ground track during the global observations phase SSTO 3.3 km

5.3 Landing Phase (LP) Trajectory Selection

The selected approach to study the landing has been using one maneuver to insert Juventas from the 2.00 km distance SSTO of the Proximity Observation phase into a collision trajectory with Didymoon at a relative velocity with respect to it of less or equal than 10 cm/s.

To this purpose, a grid of possible landing points in the Didymoon surface was selected. This grid has a longitude and latitude span of 10°, being the 0° longitude the meridian which crosses the Didymain-Didymoon vector in the opposite direction to Didymain. The 0° latitude is chosen to be coincident with Didymain's equator, i.e. perpendicular to its rotation axis. The positive longitudes are chosen along the direction of Didymoon's velocity, and the positive latitudes are chosen along the Didymoon's pole direction.

Using the points of the grid and a relative velocity normal to Didymoon surface, a backward propagation was performed until either of the following two criteria was found: the distance of the trajectory to Didymain center of mass is within 2.00 ± 0.1 km, or the propagation time reached minus 12 hours.

For each trajectory reaching the 2.00 ± 0.1 km of distance, the corresponding SSTO at that distance was computed. Among all those trajectories, the landing trajectory was selected as the one that is at the minimum distance to the SSTO plane (**red** dot in all following plots).

In this approach, two parameters were varied for the different cases, the landing epoch and the relative landing velocity with respect to Didymoon surface:

- Landing epoch: 12 different landing epochs have been studied, each of them separated from the previous 1 hour. The reason below this idea is to study the landing in different Didymoon positions in its orbit which has a period of 11.92 hours.
- Landing velocity: the landing velocity was varied from 5 cm/s to 10 cm/s using a step of 1 cm/s.

5.3.1 Analysis on Touchdown Velocity

In this section a table of the main characteristics for the studied trajectories at each epoch and velocity are shown. These main characteristics involve:

- **The landing date.**
- **Feasible landing area:** this is the available Didymoon surface after subtracting those landing points that when propagating backwards crash against any of the asteroids before reaching the 2 ± 0.1 km and those landing points whose absolute landing velocity (no the relative w.r.t. Didymoon) forms an angle with the normal to the Didymoon surface less than 90 deg (because this will imply that the trajectory before reaching the landing points comes from the interior of Didymoon).
- **Minimum distance to the SSTO plane:** this is for all the trajectories studied the minimum distance to the SSTO plane (SSTO of 2 ± 0.1 km distance to Didymain center). This distance corresponds to the selected trajectory at each landing date.
- **Duration:** Duration of the landing trajectory.
- **Didymoon Phase Angle at Landing; Juventas Phase Angle w.r.t. Didymain < 90°; Juventas Phase Angle w.r.t. Didymoon < 90°:** This parameters shows if the visibility conditions are sufficient for the landing trajectory, the first of the parameters highlights the possibility of a Didymoon eclipse, the worst case condition for an eclipse is when the Sun is in the Didymoon orbital plane, assuming parallel rays from the Sun, a Didymain radii of 387.5m and a Didymoon orbit of 1.18 km, the eclipses zone will be from 160.83° to 180° of Didymoon phase angle. The other two parameters show if during the landing trajectory the phase angle w.r.t. any of the asteroids has overcome the limit of 90° (when Juventas is in the SSTO this condition cannot be fulfilled wrt. Didymain, therefore the initial point is excluded in the analysis w.r.t. Didymain).

5.3.1.1 Landing velocity 5 cm/s.

No trajectory was found to land at 5 cm/s starting at 2 ± 0.1 km from Didymain. All the trajectories crash into Didymoon or Didymain before reaching the Proximity Observations SSTO when propagating backwards from the landing points.

5.3.1.2 Landing velocity 6 cm/s.

Table 5-6 Landing study at landing velocity of 6cm/s.

Landing Date	Feasible landing area.	Minimum distance to the SSTO plane.	Duration	Didymoon Phase Angle at Landing	Juventas Phase Angle	Juventas Phase Angle wrt Didymoon
--------------	------------------------	-------------------------------------	----------	---------------------------------	----------------------	-----------------------------------

					wrt Didymain < 90°	< 90°
28-July-2027 16:15:00	6.97%	786.49m	2.25 hours	22.8°	Yes	Yes
28-July-2027 17:15:00	6.83%	916.81m	9.5 hours	12.0°	No	No
28-July-2027 18:15:00	6.69%	603.71m	6 hours	39.7°	No	No
28-July-2027 19:15:00	6.12%	3.48m	6.5 hours	69.4°	Yes	Yes
28-July-2027 20:15:00	6.12%	9.05m	7 hours	99.3°	No	Yes
28-July-2027 21:15:00	6.12%	11.03m	8 hours	129.2°	No	No
28-July-2027 22:15:00	6.26%	1206.60m	8 hours	158.3°	No	No
28-July-2027 23:15:00	6.4%	436.58m	11.5 hours	166.9°	No	No
29-July-2027 00:15:00	6.69%	512.59m	6 hours	138.9°	No	No
29-July-2027 01:15:00	6.69%	7.85m	6.75 hours	109.2°	No	No
29-July-2027 02:15:00	6.4%	13.86m	7.25 hours	79.3°	No	No
29-July-2027 03:15:00	6.4%	185.43m	8 hours	49.5°	No	No
29-July-2027 04:15:00	6.97%	584.59m	8.75 hours	20.4°	No	No

The closest trajectory to the SSTO is the one at 28-July-2027 19:15:00. However, the area of feasible landing points is quite small, therefore little errors could lead to a not desired crashing trajectory. Only two cases show enough illumination conditions.

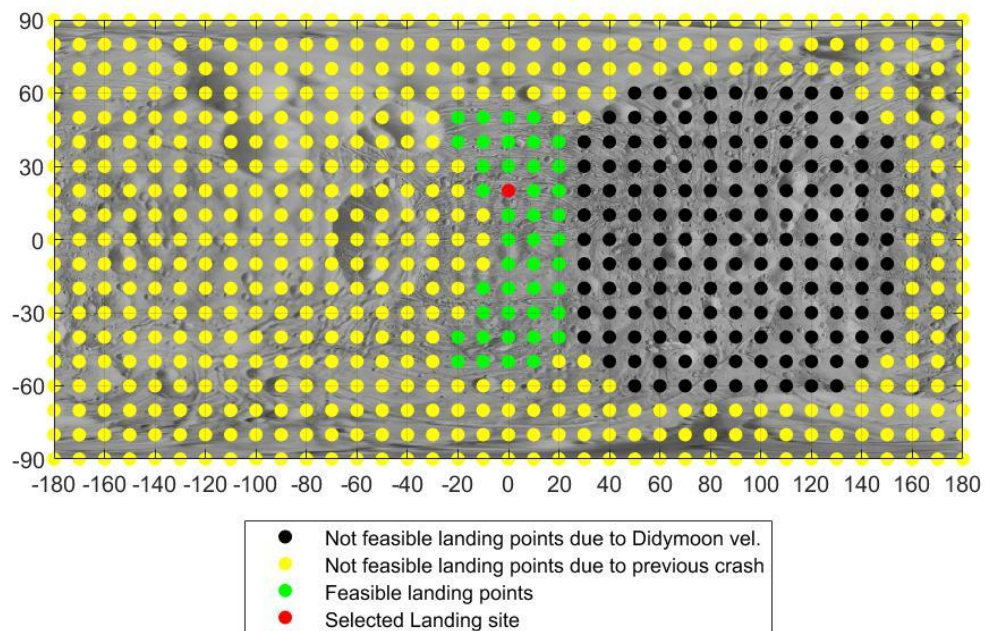


Figure 5-25 Landing Sites at a 6cm/s landing velocity at 28-July-2027 19:15:00

5.3.1.3 Landing velocity 7 cm/s.

Table 5-7 Landing study at landing velocity of 7 cm/s.

Landing Date	Feasible landing area.	Minimum distance to the SSTO plane.	Duration	Didymoon Phase Angle at Landing	Juventas Phase Angle wrt Didymain < 90°	Juventas Phase Angle wrt Didymoon < 90°
28-July-2027 16:15:00	33.71 %	80.12 m	11 hours	22.8°	No	No
28-July-2027 17:15:00	33.14%	378.76 m	5.25 hours	12.0°	No	Yes
28-July-2027 18:15:00	33 %	0.47 m	6.5 hours	39.7°	Yes	Yes
28-July-2027 19:15:00	32.29%	0.33m	8.25 hours	69.4°	Yes	Yes
28-July-2027 20:15:00	32.57%	0.46m	9 hours	99.3°	No	Yes
28-July-2027 21:15:00	33%	0.63m	11.25 hours	129.1°	No	No

28-July-2027 22:15:00	32.72%	9.01m	11 hours	158.3°	No	No
28-July-2027 23:15:00	33.43%	23.27m	10.5 hours	166.9°	No	No
29-July-2027 00:15:00	33.29%	7.23m	6.25 hours	138.9°	No	No
29-July-2027 01:15:00	33.29%	0.64m	8 hours	109.2°	No	No
29-July-2027 02:15:00	33.57%	0.16m	9.5 hours	79.3°	No	No
29-July-2027 03:15:00	33.71%	2.45m	10.75 hours	49.5°	No	No
29-July-2027 04:15:00	33.29%	261.13m	10.75 hours	20.4°	No	No

Increasing 1cm/s the landing velocity improves enormously the distance to the SSTO, however the number of feasible landing points is still very low, at around 30%. The number of cases with enough illumination conditions is the same than for landings at 6 cm/s.

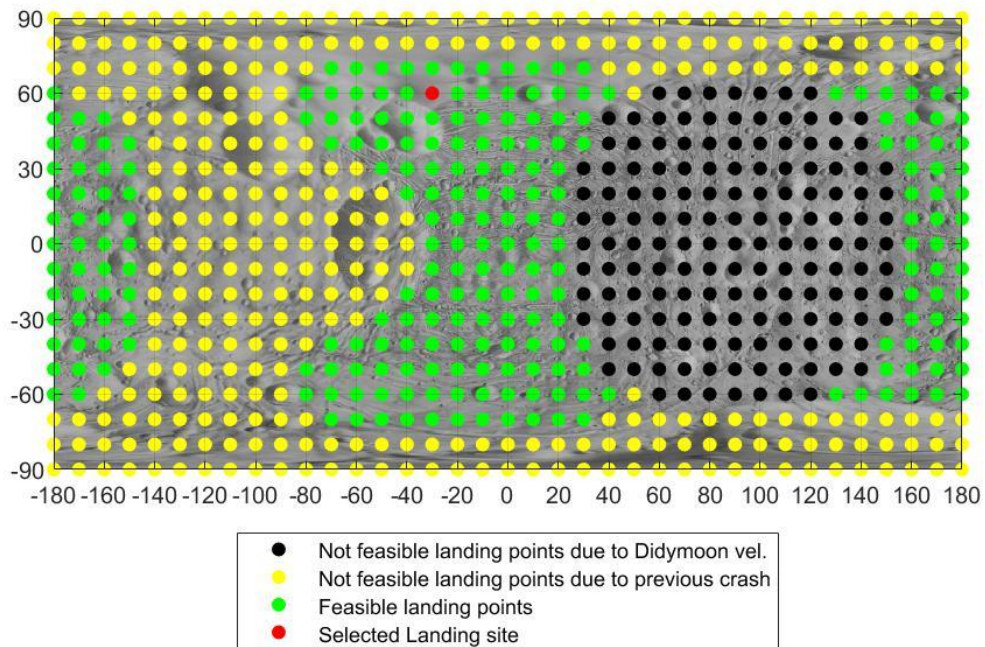


Figure 5-26 Landing Sites at a 7 cm/s landing velocity at 29-July-2027 02:15:00

5.3.1.4 Landing velocity 8 cm/s.

Table 5-8 Landing study at landing velocity of 8 cm/s.

Landing Date	Feasible landing area.	Minimum distance to the SSTO plane.	Duration of trajectory	Didymoon Phase Angle at Landing	Juventas Phase Angle wrt Didymain < 90°	Juventas Phase Angle wrt Didymoon < 90°
28-July-2027 16:15:00	51.92%	2.08m	11.5 hours	22.8°	No	No
28-July-2027 17:15:00	51.92%	0.26m	4.5 hours	12.0°	Yes	Yes
28-July-2027 18:15:00	51.64%	0.96m	6.25 hours	39.7°	Yes	Yes
28-July-2027 19:15:00	51.49%	1.39m	8 hours	69.4°	Yes	Yes
28-July-2027 20:15:00	52.06%	2.93m	11.75 hours	99.3°	No	Yes
28-July-2027 21:15:00	51.49%	0.77m	12 hours	129.1°	No	No
28-July-2027 22:15:00	51.92%	3.94m	9.25 hours	158.3°	No	No
28-July-2027 23:15:00	51.92%	0.11m	4.75 hours	166.9°	No	No
29-July-2027 00:15:00	51.92%	1.28m	12 hours	138.9°	No	No
29-July-2027 01:15:00	52.06%	0.77m	9.25 hours	109.2°	No	No
29-July-2027 02:15:00	52.49%	2.52m	12 hours	79.3°	No	No
29-July-2027 03:15:00	52.20%	4.01m	8.25 hours	49.5°	No	No
29-July-2027 04:15:00	51.64%	0.76m	11.5 hours	20.4°	No	No

Similar conclusions that for 7cm/s are obtained:

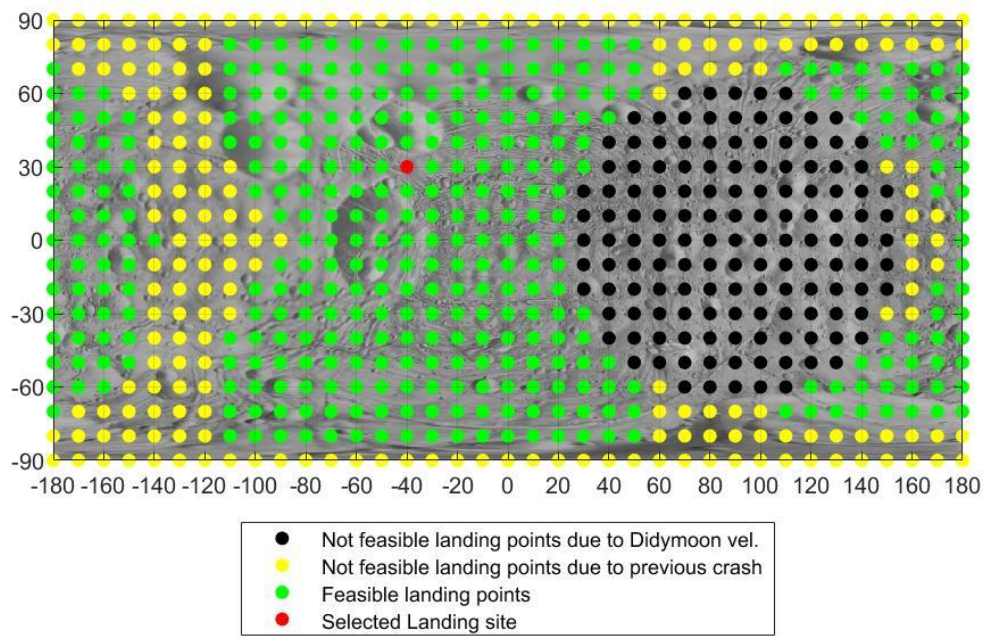


Figure 5-27 Landing Sites at a 8 cm/s landing velocity at 29-July-2027 23:15:00

5.3.1.5 Landing velocity 9 cm/s.

Table 5-9 Landing study at landing velocity of 9 cm/s.

Landing Date	Feasible landing area.	Minimum distance to the SSTO plane.	Duration of trajectory	Didymoon Phase Angle at Landing	Juventas Phase Angle wrt Didymain < 90°	Juventas Phase Angle wrt Didymoon < 90°
28-July-2027 16:15:00	72.97%	0.21 m	3.5 hours	22.8°	Yes	Yes
28-July-2027 17:15:00	72.97%	0.42 m	4.75 hours	12.0°	Yes	Yes
28-July-2027 18:15:00	72.12%	0.04 m	6.5 hours	39.7°	Yes	Yes
28-July-2027 19:15:00	71.69%	1.48 m	8 hours	69.4°	Yes	Yes
28-July-2027 20:15:00	71.55 %	0.79 m	10.5 hours	99.3°	No	Yes
28-July-2027 21:15:00	71.98%	222.55m	8 hours	129.1°	No	No

28-July-2027 22:15:00	72.12%	0.06 m	3.5 hours	158.3°	No	No
28-July-2027 23:15:00	72.69%	0.16 m	4.5 hours	166.9°	No	No
29-July-2027 00:15:00	73.12 %	1.46 m	6 hours	138.9°	No	No
29-July-2027 01:15:00	72.97%	4.82 m	9.5 hours	109.2°	No	No
29-July-2027 02:15:00	72.69%	2.45 m	10 hours	79.3°	No	No
29-July-2027 03:15:00	72.69%	271.3 m	8.25 hours	49.5°	No	No
29-July-2027 04:15:00	72.97%	0.21 m	3.5 hours	20.4°	Yes	Yes

At 9 cm/s the feasible landing area is highly increased, leading to an acceptable 70%, and except for two cases, all the distances to the SSTO are below 5m and most of them (7/12) are below 1m. Moreover, 5/12 cases show enough light.

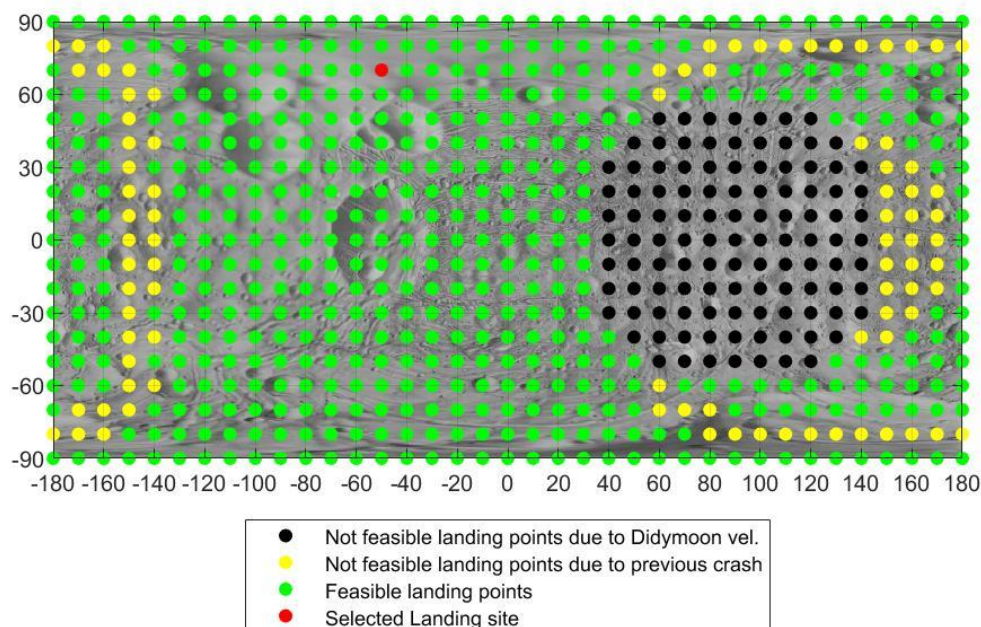


Figure 5-28 Landing Sites at a 9 cm/s landing velocity at 28-July-2027 18:15:00

5.3.1.6 Landing velocity 10 cm/s.

Table 5-10 Landing study at landing velocity of 10 cm/s.

Landing Date	Feasible landing area.	Minimum distance to the SSTO plane.	Duration of trajectory	Didymoon Phase Angle at Landing	Juventas Phase Angle wrt Didymain < 90°	Juventas Phase Angle wrt Didymoon < 90°
28-July-2027 16:15:00	77.38%	0.83 m	3.5 hours	22.8°	Yes	Yes
28-July-2027 17:15:00	77.95%	0.54 m	4.5 hours	12.0°	Yes	Yes
28-July-2027 18:15:00	77.67%	5.65 m	9 hours	39.7°	Yes	Yes
28-July-2027 19:15:00	76.67 %	3.68 m	8.25 hours	69.4°	Yes	Yes
28-July-2027 20:15:00	75.82%	2.58 m	10 hours	99.3°	No	Yes
28-July-2027 21:15:00	75.96%	131.51m	11.5 hours	129.1°	No	No
28-July-2027 22:15:00	76.24 %	0.59m	2.75 hours	158.3°	No	No
28-July-2027 23:15:00	76.67 %	0.99 m	11.25 hours	166.9°	No	No
29-July-2027 00:15:00	76.10 %	5.72 m	6 hours	138.9°	No	No
29-July-2027 01:15:00	75.82 %	2.47 m	8.75 hours	109.2°	No	No
29-July-2027 02:15:00	76.96 %	1.91 m	11.25 hours	79.3°	No	No
29-July-2027 03:15:00	77.24 %	19.67 m	10.75 hours	49.5°	No	No
29-July-2027 04:15:00	77.52 %	0.49 m	3 75 hours	20.4°	Yes	Yes

The percentage of feasible landing area is hardly increased with respect to the 9 cm/s. Besides, only 5/12 of the epochs show a minimum distance to the SSTO below 1m, while for 9 cm/s there were 7. Finally, there is no improvement with respect to the illumination conditions.

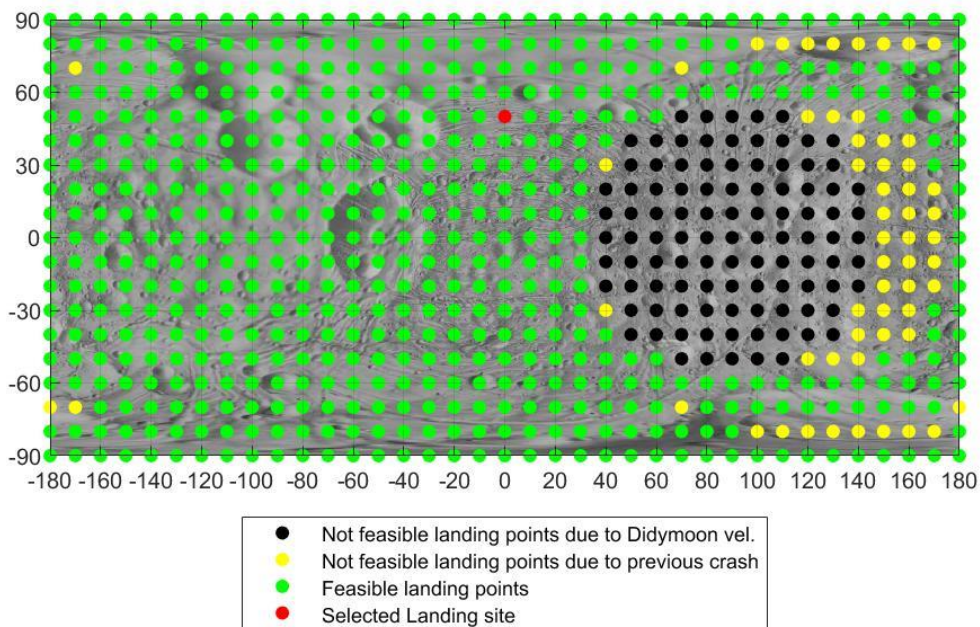


Figure 5-29 Landing Sites at a 10 cm/s landing velocity at 29-July-2027 04:15:00.

5.3.2 *Landing Trajectory*

As it can be appreciated, the feasible landing area is increased with the landing velocity. Nevertheless, this increase is not very significant between 9 and 10 cm/s. Selecting a low velocity implies that only a small section of Didymoon surface is available from the SSTO, therefore velocities below 8 cm/s are discarded.

With respect to distance to the SSTO, in the last two cases it can be observed how this distance is worsen at the same epochs: 28-July-2027 21:15:00 and 29-July-2027 03:15:00. However, this trend is not observed in the rest of the velocities, what is indeed observed is that for low velocities (6 and 7 cm/s), the distances are clearly worse, reinforcing the idea of discarding these velocities for landing.

The landing trajectory duration does not seem to have a clear relationship with either the velocity or the landing date.

To ensure velocities below 10 cm/s according to the landing requirement, a velocity of 9 cm/s will offer a 10% threshold without compromising the extension of the feasible landing area nor the illumination conditions, and still offering low distances from the SSTO.

The selected trajectory is:

Landing date: 28-July-2027 18:15:00, velocity 9 cm/s and duration 6.5 hours, distance to the SSTO 0.4 m.

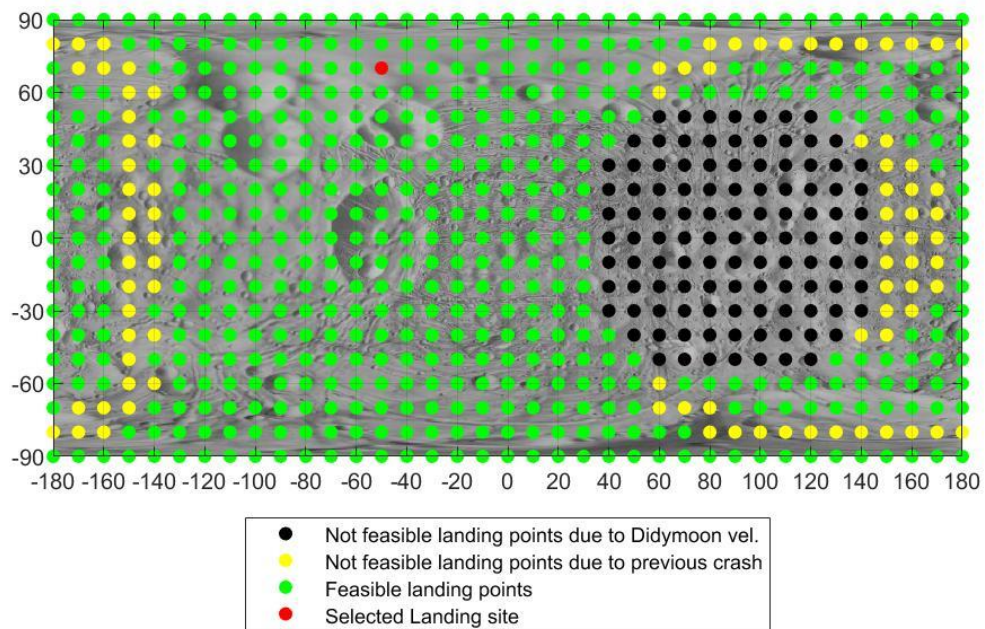


Figure 5-30 Landing Sites at a 9 cm/s landing velocity at 28-July-2027 18:15:00

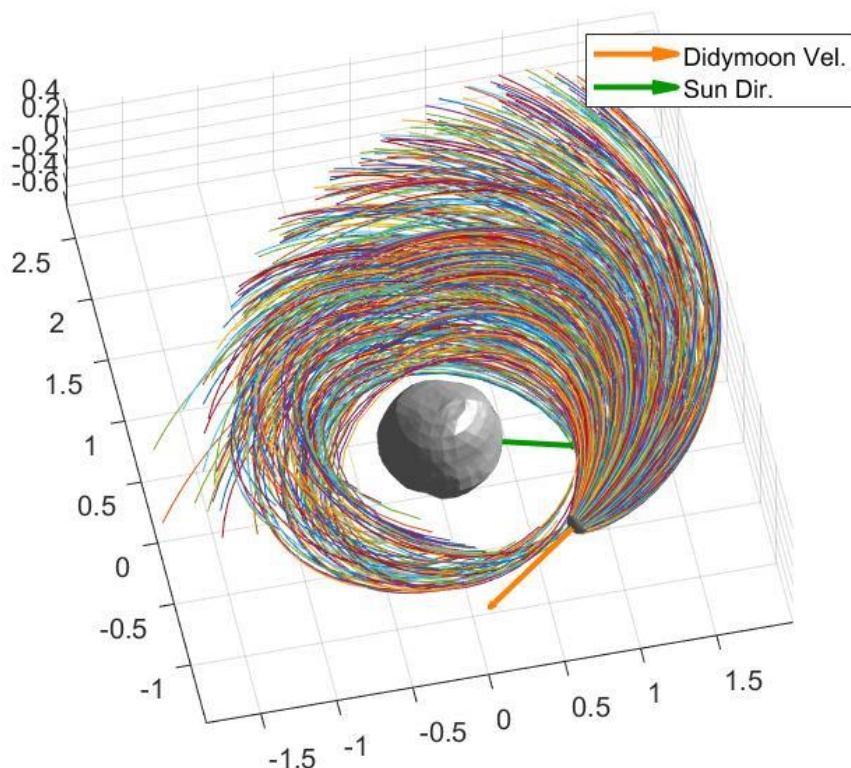


Figure 5-31 Landing Trajectories at a 9 cm/s landing velocity at 28-July-2027 18:15:00, only the 8 hours prior landing are plot.

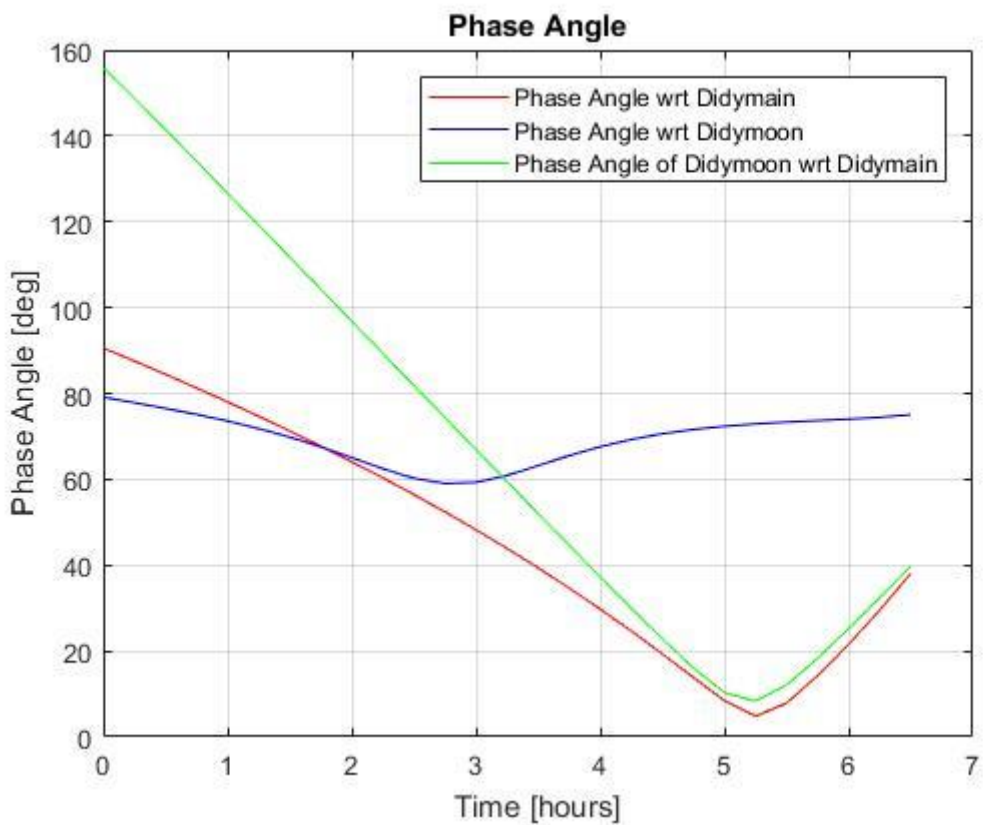


Figure 5-32 Phase angles analysis for the selected landing at a 9 cm/s landing velocity at 28-July-2027 18:15:00.

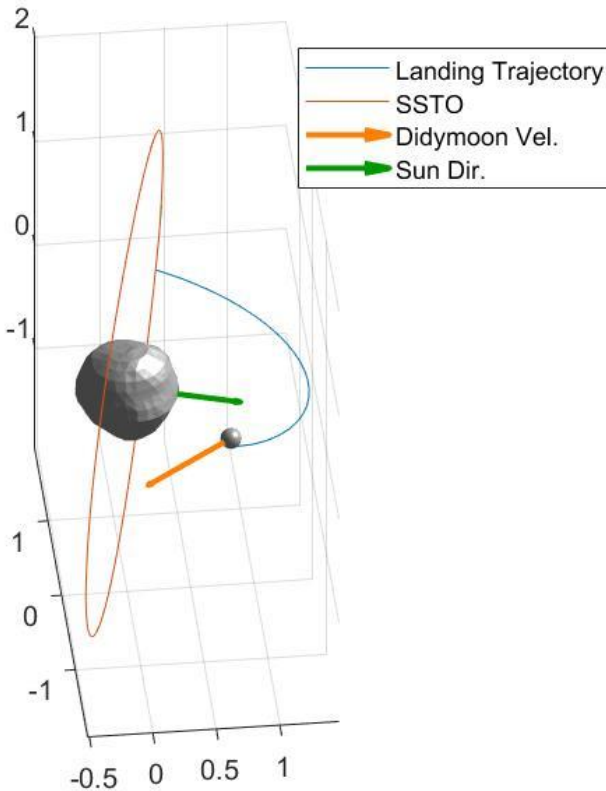


Figure 5-33 Selected landing at a 9 cm/s landing velocity at 28-July-2027 18:15:00.

If for any reason the landing date cannot be reached, similar results can be obtained, if the Sun direction has not changed significantly, waiting until Didymoon is in the same relative position w.r.t. the SSTO at the moment of the injection, this is 68.32° with respect to its previous pass to the SSTO.

5.3.2.1 Delta V

The Delta V required to inject Juventas into the previously chosen landing trajectory from the SSTO is 16.92 cm/s.

If a rehearsal is performed, assuming that Juventas is returned back to the SSTO 15 minutes before the touchdown, the total Delta V of the rehearsal accounting for the injection from SSTO to landing, the maneuver to return to the SSTO distance, and the maneuver to insert Juventas into the SSTO, is 76.16 cm/s.

Thud, the Delta V budget required to perform one rehearsal and the final landing injection is below the 1 m/s, fulfilling with the Delta V budgeted for the landing phase (assuming 100% of margin, since the Delta V allocated for landing is 2 m/s).

5.3.2.2 Bounces

Since the mechanical properties of the surface are unknown is important to determine the possibility of losing the CubeSat after the initial touchdown and rebound due to a collision with Didymos or an escape of the system. To do so, the CoR (coefficient of restitution) must be taken into account, this is the ratio of the incoming to outgoing velocity during the rebound event.

Since the real CoR is ignored, a simulation was performed using each CoR from 1 to 0.05 with a step of -0.05. This simulation consisted in propagating each feasible landing point, using an initial velocity in the

same direction but opposite sense than the landing one (this is, normal to the Didymoon surface), and with a value that is the result of multiplying the landing velocity times the CoR. These propagation lasts until a collision with any of the asteroids takes place or 12 hours after the landing.

The maximum CoR which enables a new collision against Didymoon is saved. This gives an idea of the worse surface conditions that would still allow a new touchdown, because the higher the CoR is, the higher outgoing velocity, therefore the higher the probability of the CubeSat to escape the system or to collide against Didymain. A high CoR means that the landing point is robust enough to allow a new rebound of Juventas in Didymoon, while a low CoR means that the landing point is less robust, increasing the probability of Juventas not landing and resting on the Didymoon surface. It is important to notice that new rebounds are more robust since the outgoing velocity is decreased after each rebound. Below it can be seen the results of the simulation for the landing at 9 cm/s at 28th of July of 2027 at 18:15:00.

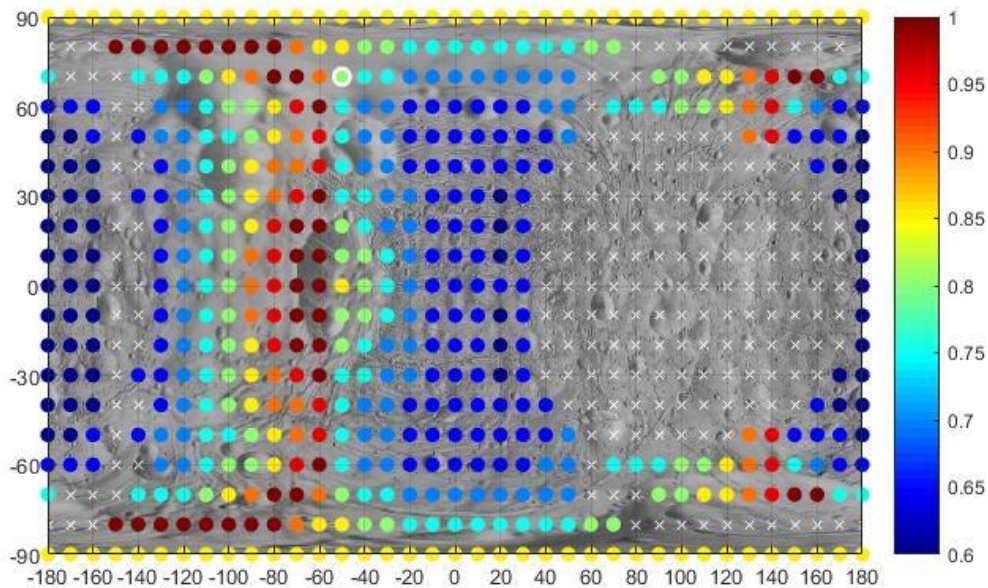


Figure 5-34 Maximum CoR allowed to ensure a future rebound in Didymoon surface after the initial landing touchdown for the landing at 9 cm/s at 28-July-2027 18:15:00.

Not feasible landing points are marked with white crosses, the selected landing point is marked with a white circle around its color marker. It can be seen how the maximum allowed CoR is distributed symmetrically around the equator due to the symmetric dynamics of the system. Most of the area with positive longitudes shows a relatively low CoR, which is in line with the fact that this area is the one which goes in the Didymoon orbital velocity sense. While the highest CoR are mostly placed in the negative longitude areas. For some points even a perfect inelastic surface is allowed (i.e. CoR =1), while the minimum CoR found is 0.6, which has been accepted as valid for MASCOT-2 studies [RD-8]. The selected landing point has a maximum CoR of 0.8. This value is high enough to assess the selection of this point. In fact, according to various studies about Didymos the expected CoR is below this number, for instance 0.6 [RD-8] and [RD-9].

The rebound trajectory for the maximum CoR allowed for the selected landing trajectory is shown below:

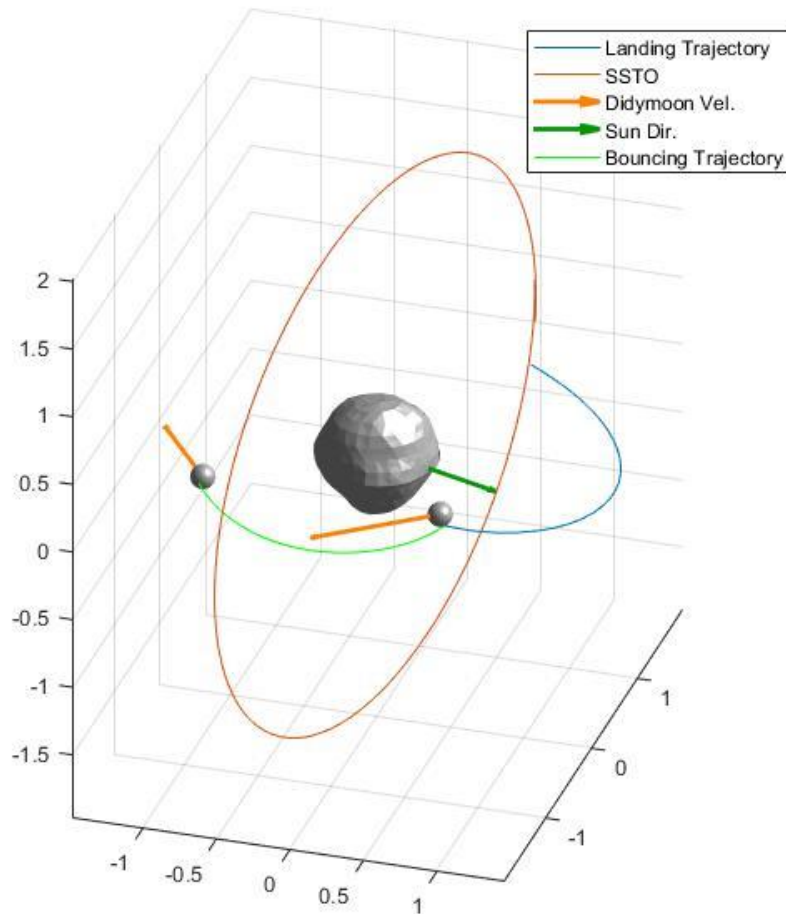


Figure 5-35 Selected landing at a 9 cm/s landing velocity at 28-July-2027 18:15:00 and posterior rebound after reaching the Didymoon surface again.

5.3.2.3 Surface-Lander Interactions

The coefficient of restitution (CoR) for a cube is different than for a sphere. CoR is defined as the square root of the ratios of the restitution and impact energies. While for a sphere that is equal to the ratio of the outgoing and incoming velocities, for a cube, this is more complicated because of rotation and friction. For the landing analysis of MASCOT-2 on Didymoon the lander was modelled as a sphere. More recent study for AGEX considered a cubic lander instead of a sphere and took into account different rock models as proposed in the ESA reference model for Itokawa (These simulations were performed by S. Tardivel with the SAL software developed at the University of Colorado, in collaboration with Stefan Van Wal). In the first order, the surface gravity, shape and the surface properties are the most important parameters for the surface interactions and the bouncing. The mass of the lander does not play a role if energy & momentum conservation and free fall are considered. The landing analysis of AGEX is therefore relevant for the JUVENTAS.

In the landing analysis of AGEX and MASOCT CoR values of 0.40 and 0.60 were used as a conservative estimate regarding the bouncing on the surface. Simulations in regolith(performed by Ron Ballouz and Clara Maurel (U Maryland)) suggested effective COR) with any surface of Didymoon bounded between 0.4 and 0.6.

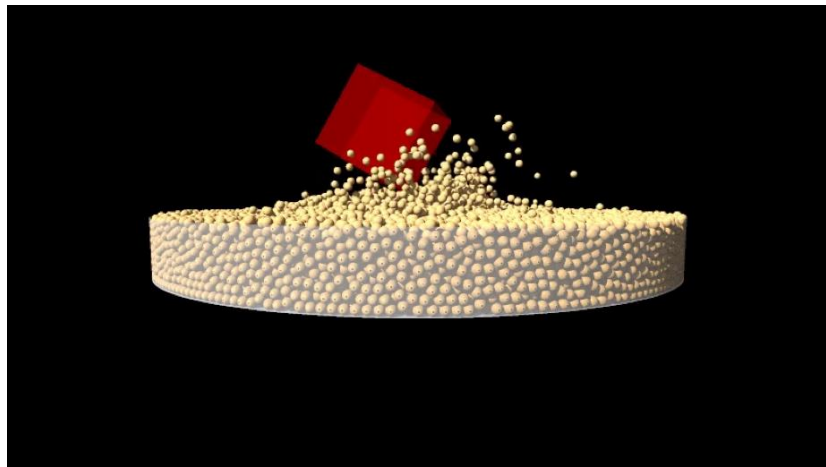


Figure 4.5 Snapshot of DEM simulation (MASCOT 2 Analysis report)

Reference Model parameters included rock models with a 'smooth' case with a rock-to-surface-ratio (RSR) = 0.19, and the 'nominal' case with a RSR = 1..9. The maximum rock diameter chosen was 2 m.

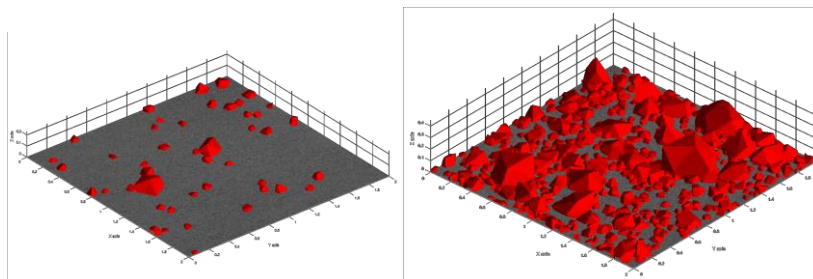


Figure XX : Reference rock models: smooth and nominal case.

The Monte-Carlo simulations yielded the mean value of less than 1 hour for the total time from touchdown to rest. Therefore power and data calculations for the AGEX mission scenario used 2 hours of bouncing as nominal values. These numbers overestimated the respective mean values by about a factor of 2, but cover most of the spread and can therefore be considered as conservative values. The bouncing behavior is different for the two rock models. For the smooth case the bouncing duration can go up to almost 8 hours in worst case..

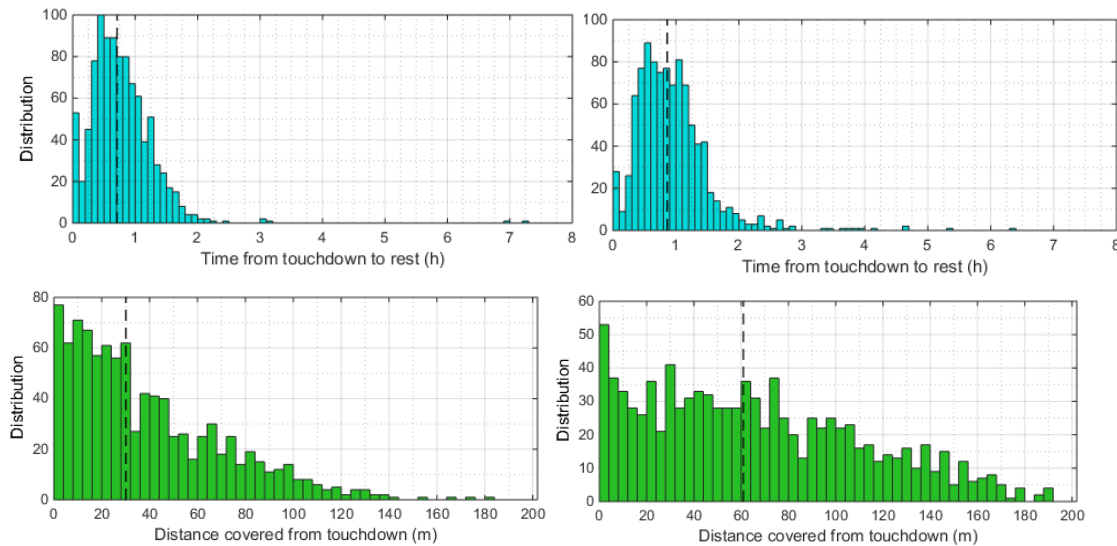
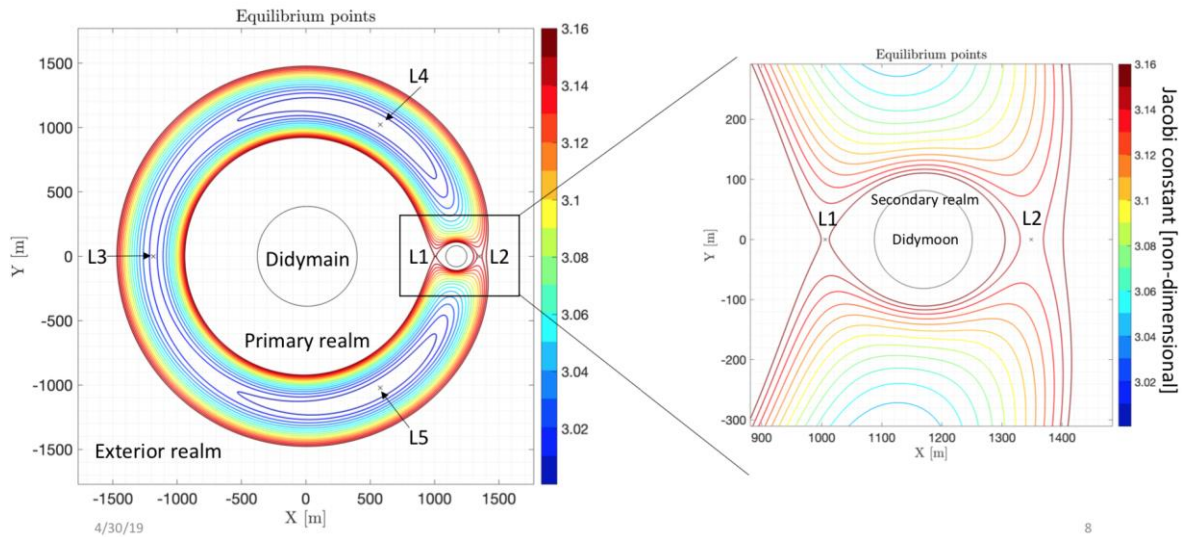


Figure XX : Simulated time from touchdown to rest (upper row) and distance covered (lower row) for the nominal (left) and the smooth (right) rock model cases

The CubeSat is expected to bounce around 30 to 40 times before it comes to rest. From these bounces, roughly the first 10 bounces can be considered important regarding the final landing location. During the bounces the distance that the CubeSat covered on the surface of Didymoon is in average around 30m and 60 m. In the smooth case, the CubeSats travel further up to 200 m.

5.3.2.4 Note on “escape velocity”

The escape velocity is calculated considering 3-body effects (i.e. opening/closure of L1 and L2 necks as a function of the lander kinetic energy). The system can be studied (Celik et al. 2018) used the circular restricted three-body problem (CR3BP) which considers gravitational attraction of both asteroids and their mutual orbit around the system barycenter (Celik et al. 2018). CR3BP admits an energy-like conserved quantity, called Jacobi constant. It is not exact equivalent of the energy, but helps understanding admissible regions of motion of spacecraft. Didymos exhibits five equilibrium points where gravity, centrifugal and Coriolis accelerations all cancel out each other



8

Primary, secondary and exterior realms are connected through “bottleneck” regions of around Lagrange points. L1 point has lower energy level (i.e., higher Jacobi constant), therefore opens up first and connect primary and secondary realms. Next is L2 point, which allows a connection between all realms. Therefore, if a spacecraft positioned beyond L2 has lower energy than that of L2 point, it can safely move in its natural course without a risk of hitting one of the asteroids. In forbidden regions, natural motion is not possible for given Jacobi constant. On the other hand L2 point is the lowest energy gate to the vicinity of Didymoon. But transferring through L2 neck also means allowing natural motion between Didymoon and Didymain,. Therefore initial Jacobi constant that is used to transfer to Didymoon vicinity must be reduced below that of L1 point to ensure staying around Didymoon.

The L1 (resp. L2) escape speed of a given point is defined as the smallest speed that opens the zero-velocity surfaces at L1 (resp. L2). The L1 (resp. L2) escape speed for a body is defined as the smallest L1 (resp. L2) escape speed across its surface.. Because L1 always opens before L2, the most conservative escape speed that can be taken is to consider the L1 escape speed. This can be summed up, rigorously, as: “After first impact, the lander must have energy less than the potential energy at L1”. The L1 escape speed for Didymoon with the current model is 4.418 cm/s and the L2 escape speed for Didymoon with the current model is 4.854 cm/s.’

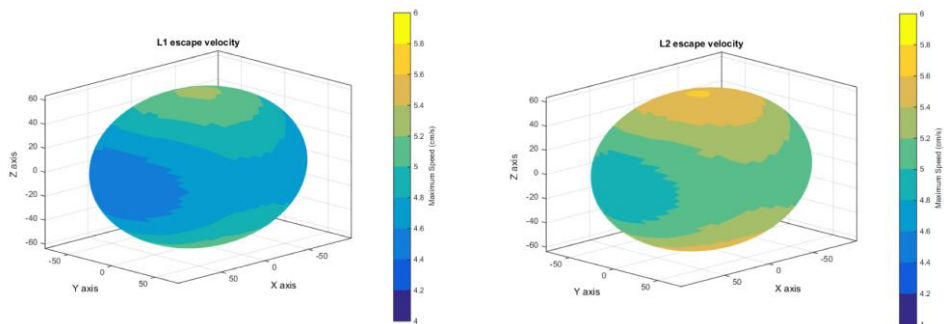
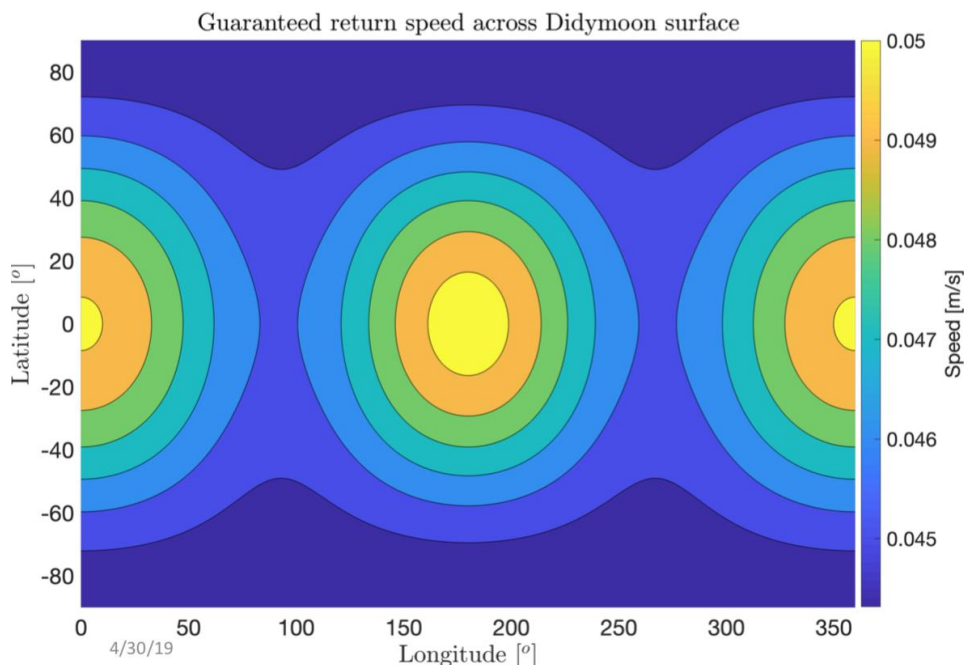


Figure 3: Escape speeds at L1 and L2 over the surface of Didymoon (courtesy of Simon Tardivel).

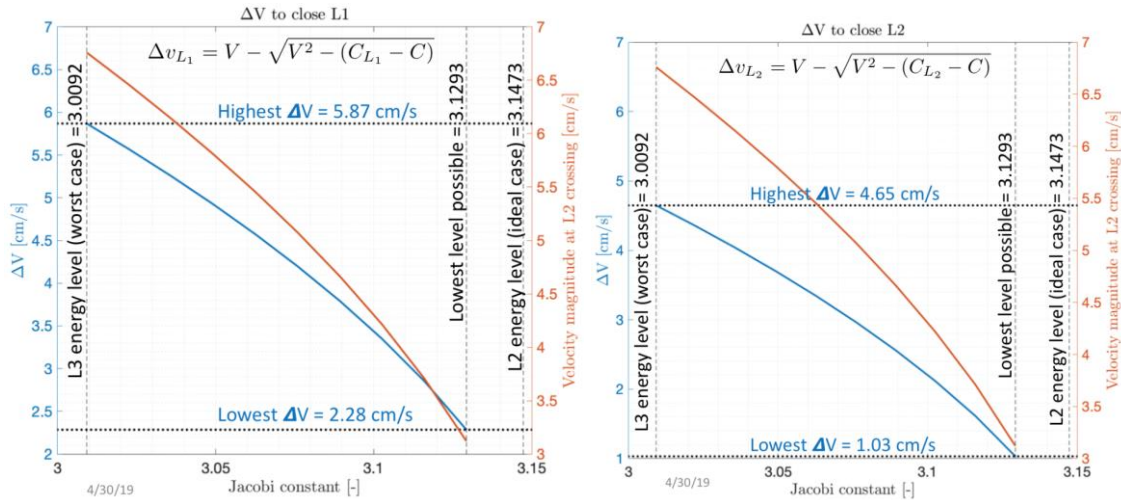
The guaranteed return speed (GRS) is a property in a three-body system to assess possibility of escape from the realm that a particle is in. It can be computed via Jacobi constant of the Lagrange point of interest. (CL) and effective potential U (gravity + centrifugal) as $v = \text{Sqrt}(2U - CL)$.

Lower than or equal to GRS, a particle will stay around its realm (e.g. Didymoon) and eventually hit the surface as result of natural motion. Hence, it can be used as an upper boundary for impact speed. While speeds below v guarantee not escaping from the system, speeds above v do not guarantee escaping the system, but merely state that a particle has enough energy to leave the realm it is in. Hence the guaranteed return speed provides the necessary condition for escape, but not the sufficient.



Minimum GRS across Didymoon surface is ~ 4.43 cm/s. Below this value, no particle can escape the vicinity of Didymoon. Accordingly, this value can be used as maximum impact speed, or maximum post-impact speed, after the first impact. Note that as three-body systems are highly nonlinear, actual conditions for escape require numerical simulations.

It is possible to control the speed during the landing, after crossing L2 distance towards Didymoon, spacecraft “energy” can be reduced before crossing L1 distance to trap the natural motion around Didymoon. Required velocity change at L2 crossing to constrain the motion in the vicinity of Didymain and Didymoon (L2 closed) is between 1.03 cm/s. and 4.65 cm/s whereas to constrain the motion in the vicinity of Didymoon only (L1 closed) is between 2.28 cm/s 5.87 cm/s.



Maximum GRS impact speed corresponds to a free-fall altitude of ~32 m (Maximum allowable free-fall altitude is ~52 m to constrain the motion in the vicinity of Didymoon). Free-fall duration varies between 14-43 min for 10-52 m altitude.

Celik, O., Sánchez, J. P., Karatekin, Ö., & Ritter, B. (2019). A comparative reliability analysis of ballistic deployments on binary asteroids. *Acta Astronautica*, 156, 308–316. <https://doi.org/10.1016/j.actaastro.2018.03.020>

Tardivel, S., & Scheeres, D. J. (2013). Ballistic Deployment of Science Packages on Binary Asteroids. *Journal of Guidance, Control, and Dynamics*, 36(3), 700–709. <https://doi.org/10.2514/1.59106>

5.4 Payload Operations Planning and Analysis

The Global Observation and Proximity Observation Phases will be focused on data acquisition of the radar and radio science experiments. An initial analysis was performed to assess the orbits for these measurements.

5.4.1 Radar Observations

The Global Observation Phase orbit of 3.3km distance SSTO was analyzed to see the impact on radar observations. The scenario analyzed was to have the radar observing for a period of 45 minutes followed by 45 minutes off, to establish a long term 50% duty cycle. During the 45 minutes of observation, the radar was transmitting 40% of the time and receiving 60% of the time. The long duration of observation is needed due to the slow relative dynamics of the Juventas SSTO orbit. Incidences were limited between 20-45 degrees. These numbers are also used to feed the power budget as indicated in the Juventas System Design Report.

The SSTO was propagated for two weeks to determine the number of revisits of radar measurements within this period. The figure below shows the revisits for Didymoon by the radar. The simulation does not take into account the shadowing of Didymain at this time. For radar tomography, it is desired to have 20 acquisitions for the 3D reconstruction. Extending the plot below shows that the 20 acquisitions can be met in just over one month, in-line with the analysis in Section 5.2.2.

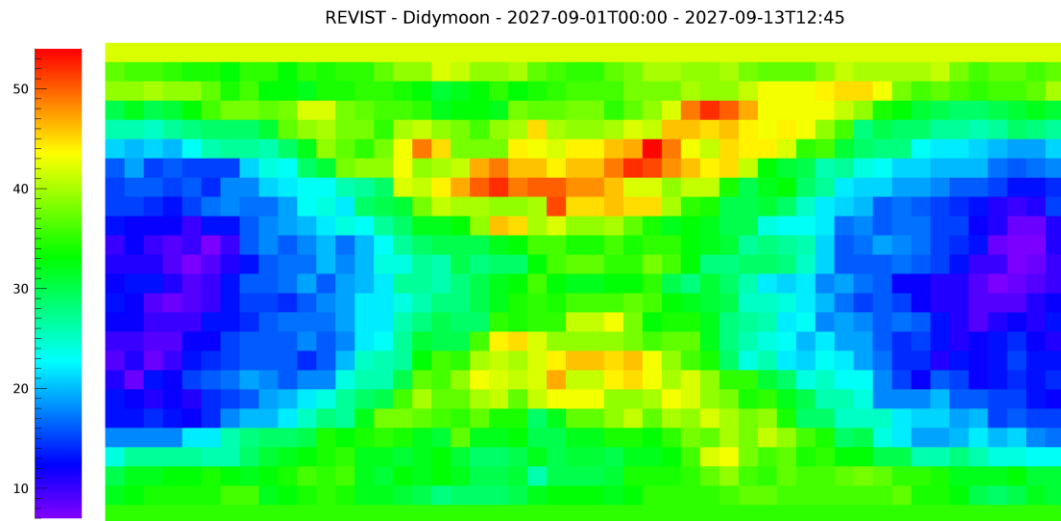


Figure 36: Radar Observation Number of Revisits across Didymoon (min=7, max=54)

5.4.2 Radio Science

The initial observation orbits have been assessed by the radar science team and have been confirmed that they are sufficient for science needs. Detailed analysis will be presented in future revisions.

5.4.3 Gravimeter

The attitude of the Juventas spacecraft after landing and bouncing events is not controlled therefore the final orientation of the spacecraft once settled on the surface is unknown for analysis. The gravimeter payload will make the most accurate measurement when parallel to the surface, however this cannot be guaranteed.

Measurements at the equator will have the largest impact on determining the dynamical state, but the landing and settling location will not be controlled.

Detailed analysis of length of expected survivability of the spacecraft on the surface for gravimeter measurements will be evaluated in future revisions. Minimum success criteria is for a single measurement requiring approximately 30 minutes of measurement time, however operation across a full Didymoon orbit period of 11.9 hours is desired to determine tidal variations.

5.5 Mission Delta-V Budget

Here below, the total delta-V for all mission phases of Juventas is shown. Two scenarios are considered, one of them represents the nominal scenario and an extra contingency case is also considered. The nominal scenario contains the standard operations conducted during the duration of each phase, while the contingency case considers rehearsals and eventual extended phases.

Table 5-11 Translational delta-V budget [cm/s] and margins as per [AD-8].

Mission Phase	Nominal Case	Contingency Case
	w & w/o 100% margin	w & w/o 100% margin

	0/0	59.4/118.8*
Release and commissioning Phase.		*This includes 5 hyperbolic arcs in total (35 days with 7-day arcs)
Transfer to SSTO.	30.5/60.9	30.5/60.9
Global Observations Phase	15/30	15/30
Transfer to Proximity Observations	5.5/11	5.5/11
Proximity Observations Phase	16.1/32.1	16.1/32.1
	16/32	76.2/152.3*
Landing Phase		*This includes landing as well as a landing rehearsal
Total	83/166 cm/s	202.6/405.2 cm/s

The total available delta-V is 10.6m/s, of which 4 m/s are used in the contingency case. Attitude maneuvers have not been included into the budget but are included in the Juventas System Design Report.

The selected baseline orbits (SSTO) need a very low delta-V for station keeping. The delta-V is computed performing maneuvers every three to four days, in groups of a week for operational simplification, which keeps Juventas in a safe corridor, 300 meters wide around the SSTO. Each maneuver is divided into two, one to perform a transfer into the SSTO and another to inject it. These two are executed together for all correction operations every three/four days. This prevents the CubeSat from leaving its orbit. If the maneuvers are scheduled every week, Juventas is not guaranteed to stay in that safe corridor. Thus, the minimum operational solution is one maneuver every 3 and 4 days. The computed delta-V needed for this station-keeping maneuvers is 7 cm/s for the GOP and 7.5 cm/s for the POP for 14 days of operations.

However, these orbits impose a quite demanding requirement on the ADCS system. Since the instruments must be pointing to either asteroid during operations, a complete rotation of the CubeSat must be performed per orbit. This will lead to very frequent saturations of the RW, thus increasing the delta-V to desaturate them. Maneuvers are executed every three to four days to keep Juventas in the SSTO. This execution should be synchronized with the RW off-loading.

Two meters per second are reserved for the landing phase, leaving room only for one landing rehearsal (considered in the contingency case).

5.6 Communication “Accesses” via ISL

Here below, a preliminary analysis on the ISL contacts between Juventas and the Hera mothercraft are shown. For both observation phases, the range between the two spacecraft is shown, and the angle between the ISL boresight and the Hera-Juventas line of sight. To be able to compute these values, it has been assumed that both phases occur at the same time of Hera’s DCP1.

Since the +Y axis of Juventas is always pointing downwards and the solar arrays and the -Z axis is always pointing to the Sun to illuminate the solar arrays, the ISL direction is contained in the SSTO plane and it remains perpendicular to the Sun direction. Since Hera always moves in trajectories with low phase angles, the LoS is on average perpendicular to the ISL boresight, with oscillations that depend on the rotation of Juventas and the current arc of Hera.

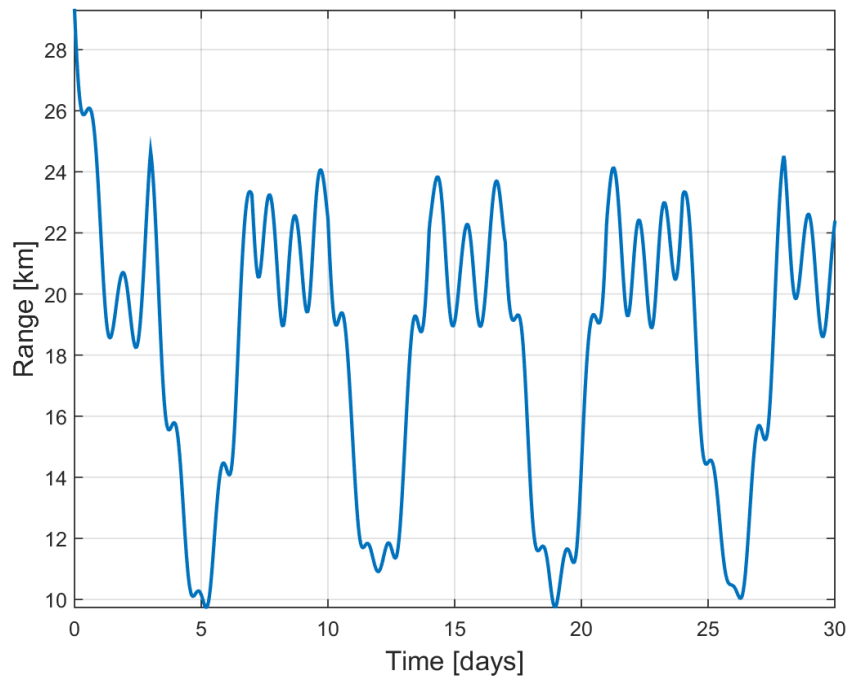


Figure 5-37 Juventas-HERA range during the GOP

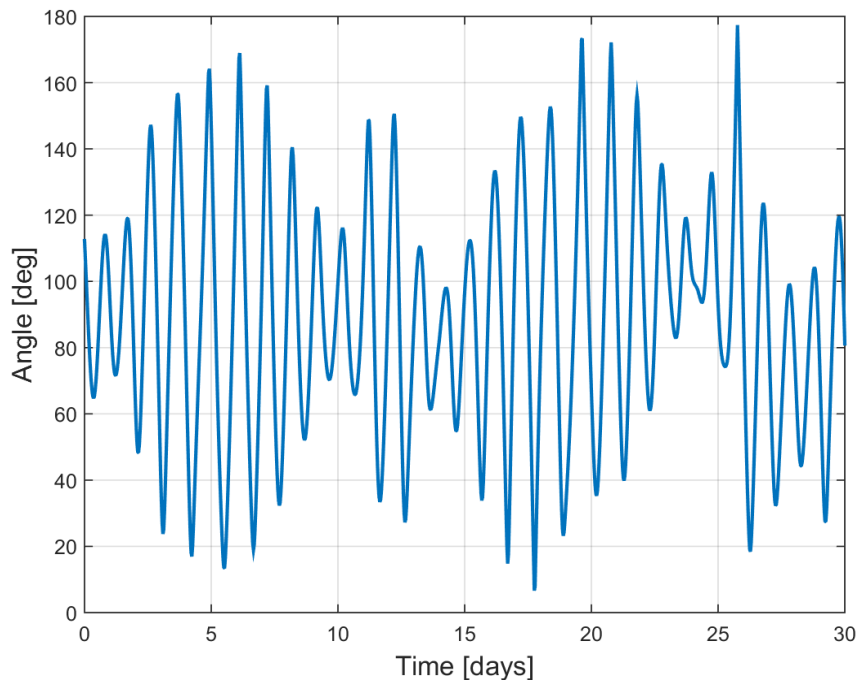


Figure 5-38 Juventas-HERA line of sight angle w.r.t ISL payload during the GOP

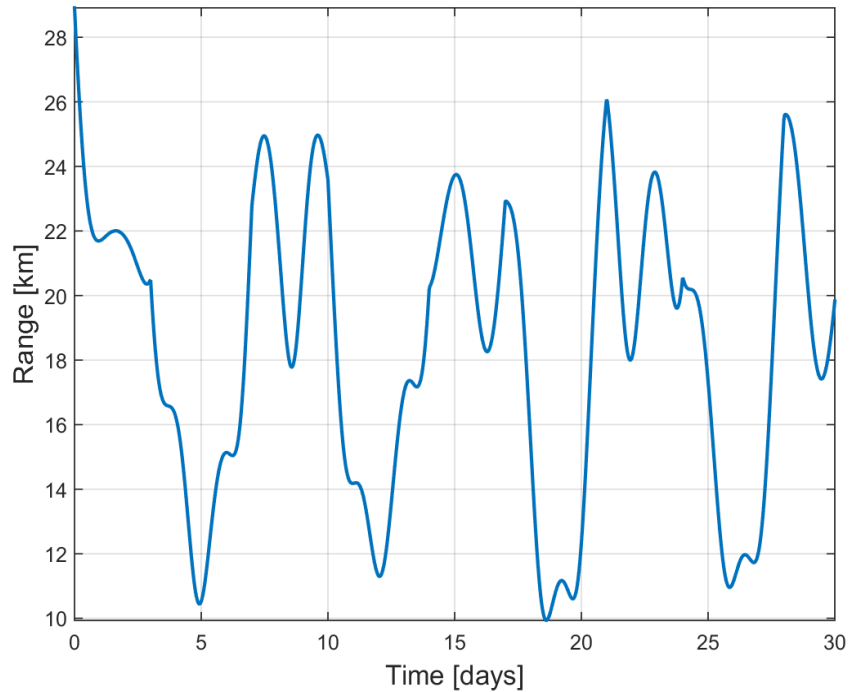


Figure 5-39 Juventas-HERA range during the POP

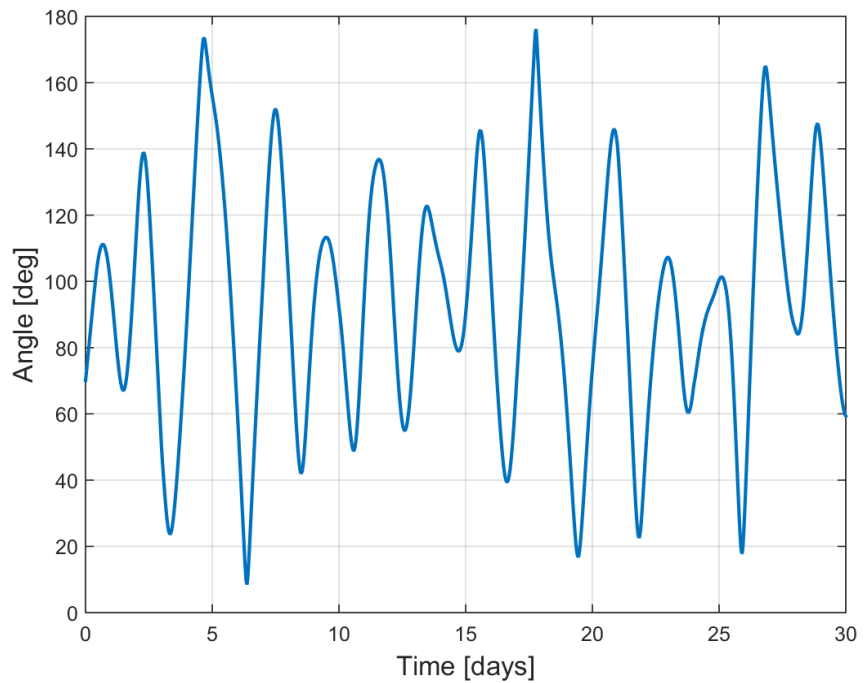


Figure 5-40 Juventas-HERA line of sight angle w.r.t. ISL payload during the POP

6. Conclusions

The initial mission analysis show feasibility of the mission design selected. Further work will refine the mission design as well as its simulation to meet science objectives within the spacecraft engineering constraints.

< End of Document >